Input-Output Metrics for the Power-Grid's Swing Dynamics

Final Project Report

S-86G

Power Systems Engineering Research Center
Empowering Minds to Engineer
the Future Electric Energy System

Input-Output Metrics for the Power-Grid's Swing Dynamics

Final Project Report

Project Team
Sandip Roy, Project Leader
Vaithianathan (Mani) Venkatasubramanian
Washington State University

Graduate Students
Mohammadreza Hatami
Kasra Koorehdavoudi
Habib Wajid
Subir Sarker
Washington State University

PSERC Publication 23-1

January 2023

For information about this project, contact:

Sandip Roy
Professor, School of Electrical Engineering and Computer Science
Washington State University
Email: sandip@wsu.edu

Power Systems Engineering Research Center

The Power Systems Engineering Research Center (PSERC) is a multi-university Center conducting research on challenges facing the electric power industry and educating the next generation of power engineers. More information about PSERC can be found at the Center's website: http://www.pserc.org.

For additional information, contact:

Power Systems Engineering Research Center
Arizona State University
527 Engineering Research Center
Tempe, Arizona 85287-5706
Phone: 480-965-1643

Notice Concerning Copyright Material

Acknowledgments

We wish to thank the industry advisors for the project, Patrick Panciatici, Florent Xavier, Gilles Torresan, and Thibault Prevost from RTE, Paris, France for their support and advice throughout the project.

Executive Summary

Part 1: Online Transfer Function Estimation and Control Design Using Ambient Synchrophasor Measurements

Power systems around the world are undergoing major changes as we transition from fossil-fuel dominated generation to intermittent renewable generation sources. Moreover, power grids are having to deal with extreme weather events and unforeseen operating conditions. In these circumstances, controller designs which are based on offline studies and detailed physical models may not be able to adjust to sudden changes in system operating conditions. This report proposes an adaptive control design framework for damping inter-area oscillations in power systems. The design is entirely based on ambient synchrophasor measurements and does not require detailed physical system models. The proposed framework consists of three components, namely, input-output transfer function estimation, channel selection, and feedback control implementation. For the first part, we propose a simple yet effective novel estimation algorithm in the frequency domain to identify low-order transfer functions in pre-specified frequency ranges between the measured input and output data using ambient synchrophasor measurements. In the second part, based on the identified transfer functions, the joint controllability-observability (JCO) of all identified channels is estimated and suitable control candidates for damping the target inter-area mode are selected. Finally, an appropriate lead-lag controller is designed using a classical frequency-domain method to improve the damping of a dominant oscillatory inter-area mode. Since ambient data is used in the analysis, the selected channel as well as the designed controller parameters can be updated online whenever the system operating point changes resulting in an efficient adaptive controller. The effectiveness of the proposed framework is illustrated by implementing it on the two-area Kundur test system.

The research developed in this project is partially described in the following paper which is under review.

Part II: Parametric Dependence Analysis and Channel Preserving Model Reduction

The design of wide-area controllers for the bulk power grid requires characterization of input-output channels in swing-dynamics models. However, the large variability in operating conditions in the modern grid makes the evaluation of channel transfer properties challenging. In this study, we examine how transfer functions in the classical swing dynamics model depend on network model parameters (the topology of line susceptances, generator inertias, dampings) and the channel location, focusing particularly on determining conditions under which the transfer function is guaranteed to be minimum phase or conversely nonminimum phase. In particular, graph-theoretic conditions as well as numerical bounds on network model parameters are obtained, that either preserve minimum-phase dynamics or yield non-minimum-phase behaviors.

Project Publications:

[1] M. Hatami, K. Koorehdavoudi, H. Wajid, V. Venkatasubramanian, P. Panciatici, F. Xavier, and G. Torresan,"Online Transfer Function Estimation and Control Design Using Ambient Synchrophasor Measurements", in review.

[2] K. Koorehdavoudi, S. Roy, T. Prevost, F. Xavier, P. Panciatici, and V. Venkatasubramanian, "Input-output properties of the power grid's swing dynamics: Dependence on network parameters," IEEE Conference on Control Technologies and Applications (IEEE CCTA), Hong Kong, 2019.

Part I

Online Transfer Function Estimation and Control Design Using Ambient Synchrophasor Measurements

Vaithianathan (Mani) Venkatasubramanian
Mohammadreza Hatami, Graduate Student
Kasra Koorehdavoudi, Graduate Student
Habib Wajid, Graduate Student

Washington State University

For information about this project, contact:

Vaithianathan (Mani) Venkatasubramanian
Professor, School of Electrical Engineering and Computer Science
Washington State University
Email: mani@wsu.edu

Power Systems Engineering Research Center

The Power Systems Engineering Research Center (PSERC) is a multi-university Center conducting research on challenges facing the electric power industry and educating the next generation of power engineers. More information about PSERC can be found at the Center's website: http://www.pserc.org.

For additional information, contact:

Power Systems Engineering Research Center
Arizona State University
527 Engineering Research Center
Tempe, Arizona 85287-5706
Phone: 480-965-1643
Fax: 480-727-2052

Notice Concerning Copyright Material

Table of Contents

List of Figures

List of Tables

1. Introduction

1.1 Background

Power system electromechanical oscillations have been a major concern for system reliability coordinators for decades. Negatively damped wide-area oscillations can lead to widespread blackouts such as was experienced on August 10, 1996 [1]-[2] in the western American interconnection. Poorly damped inter-area oscillations can be a concern for operational reliability of the system, and recent instances include the European interconnection oscillation event on December 3, 2018 [3]. Poorly damped and sustained oscillations can potentially endanger safety and longevity of expensive system components owing to fatigue and vibrations on physical quantities [4]. In general, oscillation concerns limit inter-area power transfers along tie-lines and can result in a less-economical operating system.

1.2 Overview of the Problem

A significant amount of research has been conducted in the past three decades on both monitoring [5]-[7] and control [8]-[11] of power system low-frequency oscillations. Feedback control is known to be effective in damping out system oscillations through controllers such as power system stabilizers (PSSs) [8], power electronic controllers [10], and High Voltage DC (HVDC) lines [12]. The two key elements in a feedback control scheme are the control location and the choice of feedback signal, together making a control channel. Joint controllability-observability (JCO) has been widely utilized as a measure for ranking the control channels and for choosing the best signals [10], [13]. Early research indicated that wide-area or remote measurements can be much more effective than local ones because of having higher JCO [14].

In [10], in addition to JCO, three other indices are used to determine the best control channel: right-half plane zeros for single-input single-output design and relative gain array and minimum singular value for multi-input multi-output design. An accurate and well-detailed model of the system can result in an effectively designed controller for the real system. However, relying solely on offline system dynamic models for controller design may be problematic in practice for the following reasons:

- Validating the small-signal modal properties of large interconnections in terms of the mode shape properties and their damping levels remains a challenging task even today [4].
- Dynamic models of real power systems are of very high order. For instance, the WECC dynamic model has over 40,000 states. Some of the proposed model-based controller design techniques require handling and operation of such large matrices in computationally expensive optimization problems which makes their application challenging.
- Analysis and control designs based on offline system models tend to be conservative and cannot easily adapt to real-time changes in system operating conditions.

- Detailed models of each system component are required to build the overall system model, and this is becoming challenging with growing integration of renewables with complex power electronic controls.

Phasor measurement units (PMUs) provide time-synchronized measurements throughout the system yielding a *wide-area view* of the system. This report proposes an alternate approach for online control design using available ambient PMU measurements.

Analysis of the PMU data for extracting some of the system dynamic features requires some form of a system identification procedure. Initial attempts for power system identification using system measurements can be traced back to Hauer's work [15] in the late 1970s where a software package for structural transfer function fitting to the given system frequency response was developed. Applications, limitations, and further developments of the aforementioned software package are discussed in [16]. Later, the initial output-only Prony technique was applied for input-output transfer function identification in [17]. Reference [18] extends the time-domain ARMAX model for the multiple-input multiple-output transfer function identification in power systems.

1.3 Proposed Solution

Ambient system measurements are the system responses to inherent random fluctuations of power system loads and renewable generations. In this report, such random load variations are used as independent system inputs and measurements such as tie-line flows, and bus frequencies are formulated as system outputs for estimating the small-signal input-output properties. In this context, there is no need for probing signal injections or system events. Since the ambient signals are always available under normal system conditions, the estimated model and the subsequent controller design can be updated online automatically on a regular basis and after major changes in system topology. Moreover, we show that the proposed frequency domain identification technique can estimate right plane zeros in the transfer function in a specified frequency range and this is helpful in avoiding the pitfalls of non-minimum phase control designs [10].

1.4 Report Organization

The rest of the report is structured as follows. Section II presents the proposed framework. Section III is devoted to simulations and discussions. Finally, conclusions are presented in section IV.

2. The Proposed Framework

In this section, we elaborate on the proposed framework which consists of three parts: (A) the proposed identification technique to estimate low-order transfer functions in pre-specified frequency ranges between the measured inputs and outputs signals, (B) determination of the best control channel for damping a specific inter-area mode based on the identified transfer functions, and (C) designing a simple lead-lag controller using frequency-domain method based on the identified transfer function.

2.1 Estimation Formulation

In this report, the aim is to estimate and utilize the input-output characteristics between available ambient inputs and the outputs of interest. For instance, active and reactive power load fluctuations can be natural system inputs in the context of ambient measurements. PMU measurements such as bus voltage magnitudes and phase angles, active and reactive power-flows and bus frequencies can be formulated as typical system outputs that are excited by the ambient inputs.

Small-signal formulation justifies the assumption of an underlying linear system so that superposition holds for input-output combinations. Therefore, the model estimation problem can be well-formulated simultaneously for subsets of input and output measurements. For instance, for a SVC design, the required input signal would be the reactive power injection at the bus which is equivalent to the reactive power load variation which is an available input to the system ambient response. Similarly, if a controllable storage device is available at the bus, the transfer function related to the active power input at that bus may be of interest as well. In other words, *any device that can control active or reactive power injection at a bus can be formulated as a candidate choice for the ambient transfer function estimation method proposed in this report.*

2.2 Transfer Function (Matrix) Identification

In this part, we present the proposed technique for identifying transfer functions between the measured input and output signals. When deriving the system properties from the system time-domain measurements, ARMAX [18] and Subspace State-Space Identification (SSI) [19] have been used in the past [20] for obtaining a reduced-order model for the system from measurements. In most identification techniques, a full state-space model, or a full transfer function (over the entire frequency band) is estimated. From there, one can examine the system characteristics near the frequency of a mode of interest. However, there are major challenges for implementing ARMAX and SSI such as the choice of the model order which has a significant impact on estimation accuracy and the presence of spurious modes [18],[19].

If the system frequency response is given, there are so many techniques to fit a transfer function to the frequency response data (e.g., [15], [16], [21]). However, in real power systems, the frequency response of a specific channel cannot be determined at present unless some probing tests are conducted.

The identification technique we propose here is based on the input and output data and does not require the knowledge of frequency responses. Here, the idea is to estimate second-order transfer functions between the available input and output data in a limited pre-specified range of frequency where there exists a known system dominant mode of interest. The significance of the mode can be confirmed, and its approximate frequency can be obtained from the output signals spectrum. The reason we can employ only a small range of frequency over the entire frequency range is that the modal information (i.e., the frequency and the damping of a mode) as well as the controllability-observability characteristic of the channels can be extracted from a neighborhood range of the mode frequency where most of the mode energy is concentrated.

Let us assume that M ambient input signals and N ambient output signals are measured by PMUs. As mentioned before, by inputs, we mean active and reactive load variations and by outputs, we mean all dependent quantities such as bus voltage magnitudes or angle differences, active or reactive line currents and line power-flows.

Let us assume a second-order continuous-time transfer function $\mathrm{H_{i,m}(s)}$ between the $\mathrm{m^{th}}$ input and the $\mathrm{i^{th}}$ output as follows.

$$\mathrm{H_{i,m}(s)} = \frac{\mathrm{d_{i,m}s^2 + \alpha_{i,m}s + \beta_{i,m}}}{\mathrm{s^2 + \sigma s + \Omega}} \tag{1}$$

where σ and Ω parameters describe the target inter-area mode and are common between different input-output pairs, whereas the $\mathrm{d_{i,m}}$, $\alpha_{\mathrm{i,m}}$ and $\beta_{\mathrm{i,m}}$ parameters are specific to each channel, and therefore signify input and output relationships. We note that the d parameter is included in the numerator since the feedforward matrix D entries are non-zero for most of the channels. In general, the overall transfer function is not of order two and what we have considered here approximates the overall transfer function in the vicinity of a dominant mode frequency, where it is assumed that no other mode has a significant effect on the mode of interest. The formulation can be readily extended to handle higher-order transfer function formulations, though it is not shown here due to space limitations. Then, the system outputs can be represented as follows.

$$\mathrm{Y_i(s)} = \sum_{\mathrm{m=1}}^{\mathrm{M}} \frac{\mathrm{d_{i,m}s^2 + \alpha_{i,m}s + \beta_{i,m}}}{\mathrm{s^2 + \sigma s + \Omega}} \mathrm{U_m(s)} \quad \text{with} \quad \mathrm{i = 1,2,\dots,N} \tag{2}$$

In the above equations, $\mathrm{Y_i(s)}$ and $\mathrm{U_m(s)}$ are the Laplace transform of the $\mathrm{i^{th}}$ output and the $\mathrm{m^{th}}$ input signals, respectively. Let us rewrite the above equations in the Fourier domain for the specific frequency range $\omega_1 < \omega < \omega_2$ around the mode of interest as follows.

$$\mathrm{Y_i(j\omega)} = \sum_{\mathrm{m=1}}^{\mathrm{M}} \frac{\mathrm{j}\alpha_{\mathrm{i,m}}\omega + \left(\beta_{\mathrm{i,m}} - \mathrm{d_{i,m}}\omega^2\right)}{\mathrm{j}\sigma\omega + (\Omega - \omega^2)} \mathrm{U}_m(\mathrm{j}\omega) \quad \text{with} \;\; \mathrm{i = 1,2,\dots,N} \quad \& \quad \omega_1 < \omega < \omega_2 \tag{3}$$

For notational convenience, we will drop $\mathrm{j}\omega$ in $\mathrm{Y_i(j\omega)}$ and $\mathrm{U_m(j\omega)}$ for the rest of derivations.

Solving the above set of equations as in (3) requires solving a nonlinear least-squares problem which by itself requires the initial values for all the parameters and may lead to multiple (local) solutions. We propose to do a cross-multiplication and restate the equation as follows.

$$\mathrm{j}\sigma\omega Y_i + (\Omega - \omega^2)Y_i = \sum_{m=1}^{M} \mathrm{j}\alpha_{i,m}\omega U_m + \sum_{m=1}^{M} (\beta_{i,m} - d_{i,m}\omega^2)U_m \qquad \text{with } i = 1,2,\ldots,N \quad \& \quad \omega_1 < \omega < \omega_2 \tag{4}$$

By rearranging the equations and putting all the unknown terms on the left and the known term on the right, we get:

$$(\mathrm{j}\omega Y_i)\sigma + (Y_i)\Omega - \sum_{m=1}^{M} (\mathrm{j}\omega U_m)\alpha_{i,m} - \sum_{m=1}^{M} (U_m)\beta_{i,m} + \sum_{m=1}^{M} (\omega^2 U_m)\, d_{i,m} = Y_i\omega^2 \qquad \text{with } i = 1,2,\ldots,N \quad \& \quad \omega_1 < \omega < \omega_2 \tag{5}$$

Now, we have a set of linear equations that can be solved as a simple linear least-squares problem. Remark 1: By doing the cross-multiplication, we are introducing a frequency-dependent weighting function to the original problem as follows:

$$min \underbrace{\|Y.Den - Num.U\|^2}_{\text{after cross-multiplication}} = min \underbrace{\left\| Y - \frac{Num}{Den}U \right\|^2}_{\text{original formulation}} . \underbrace{|Den|^2}_{\text{weigting}} \tag{6}$$

where, $Den = \mathrm{j}\sigma\omega + (\Omega - \omega^2)$ is the common denominator of all channels and Num is the numerator of the transfer function. By its nature, Den gets very small values as ω approaches the mode angular frequency and gets higher values as ω approaches ω_1 and ω_2. This means that less importance will be given to equations around the mode frequency and more will be given to equations at the two sides of the frequency range. Since the mode damping is dominantly correlated by the changes of transfer function magnitude around the mode frequency, this weighting function will bias the mode damping estimates. To overcome this problem, we propose the following steps:

1) Estimate the transfer function parameters by solving (5).
2) Build the frequency-dependent weighting function $\widehat{Den} = \mathrm{j}\sigma\omega + (\Omega - \omega^2)$ using the estimated σ and Ω parameters.
3) Estimate the transfer function parameters again by solving (5) with including a frequency weighting function $\frac{1}{\widehat{Den}^2}$ where $\widehat{Den}$ is built in Step 2. This will counter the effect of the natural weighting Den^2 to a great extent.

As an alternative, one can use the σ and Ω from the previous window estimation (please note that we are performing a moving window analysis) to create $\widehat{Den}$ and solve (5) by considering the weighting function $\widehat{Den}$ from the beginning.

2.3 Input-Output Channel Selection

When employing a feedback controller to damp out the system oscillations, three factors are of importance, that is, the control location, the feedback signal, and the designed controller by itself. The first two factors are associated with the controllability and observability, respectively. The best input-output channel for control implementation has the highest joint controllability-observability [10], [13], and [14].

In the power system literature, three different approaches can be found addressing the joint controllability-observability problem.

The first approach evaluates the joint controllability-observability based on the Hankel Singular Values (HSVs) which are defined as $\sigma_i = \sqrt{\lambda_i(PQ)}$ where $i = 1, \dots, n$ and P and Q are the controllability and observability grammarian matrices, respectively, and n is the order of the system. The channel with higher HSV has higher JCO [10].

The second approach, known as the "geometric" measure [13], defines the controllability index as $\left|q_i^T b_j\right| / \left(\|q_i\| \left\|b_j\right\|\right)$, where q_i is the left eigenvector associated with the i^{th} mode and b_j is the column vector of the input matrix B associated with the j^{th} input. Similarly, the observability index is defined as $\left|c_k^T p_i\right| / (\|c_k\| \|p_i\|)$, where p_i is the right eigenvector associated with the i^{th} mode and c_k is the k^{th} row of the output matrix C associated with the k^{th} output. One advantage of this method is that the indices from different physical quantities (with different units) can be compared together, due to the normalization placed in the denominator [11].

The third approach is based on the partial fraction expansion of different channels transfer functions, where the channel with higher residue at the mode of interest has higher joint controllability-observability [13], [14]. In fact, it is shown in [13] that the residue $R_{k,j}$ associated with the j^{th} input and the k^{th} output is related to the $A, B,$ and C matrices as $R_{k,j} = c_k p_i q_i b_j$. As mentioned in [13], when the inputs are of the same type, the normalization by $\left\|b_j\right\|$ in the denominator of $\left|q_i^T b_j\right| / \left(\|q_i\| \left\|b_j\right\|\right)$ should be removed as it shows the power injected by the input to the system. A similar discussion can be made for the observability measure. Moreover, it is mentioned that when examining the joint controllability-observability, the normalizations by $\|q_i\|$ and $\|p_i\|$ can be removed as the different choice of state similarity transformations will be canceled out in their multiplications. In other words, if the inputs are of the same type (outputs as well), the residues from transfer function expansion and the "geometry" measure defined in [13] will be equivalent. To obtain the JCO of each channel, we will do partial fraction expansion on each channel's identified transfer function and obtain the residues. The channel with highest residue has highest JCO and therefore most suitable for feedback control implementation.

2.4 Feedback Controller Design

After selecting the best input-output channel in the previous part, a feedback controller should be designed to effectively damp out the inter-area oscillations. Since the system identification is performed in the frequency domain, it is a natural choice to design the controller in frequency domain as well. Numerous techniques have been used in power system literature (e.g., [22], Chapter 17). In this work, we will use the bode plot-based lead-lag compensator where the controller is updated as the system operating point changes with time. This will make the control adaptive in nature, thus capable of tracking changes in system conditions and providing proper stabilization as needed.

For the sake of space, we will not present the complete classical feedback lead-lag controller design in detail and we refer readers to [23], Pages 751 to 757 for details. A small overview will be presented here though. In this report, for the system open loop identified transfer function and the feedback controller we will use the notations, G(s) and H(s), respectively. First, the phase margin of open loop system is assessed from the identified frequency response at the mode of interest. Then, an appropriate amount of phase is added to this using a series compensator, centered around the mode of interest, to bring the phase margin of the closed loop system to a desired value. An additional amount of phase is also added to accommodate for the change in phase margin of closed loop system, due to the gain of controller, this is referred to as safety margin in the literature. Moreover, the center frequency of compensator is set slightly higher than the frequency of the mode of interest. This accommodates for the change of gain crossover frequency due to the feedback controller and results in much less controller phase and gain to be created. Depending on the total amount of phase contribution to be achieved, the number of compensator stages is determined such that maximum phase of each stage is limited to 60°.The magnitude of controller is chosen so that its gain contribution is minimal at the mode of interest. Finally, the response of the closed loop system is observed for the updated phase margin. Frequency response-based controller design is an iterative procedure widely used in the industry, and maybe repeated until the desired stability margins are achieved.

3. Simulation and Results

In this section, the effectiveness of the proposed framework is demonstrated using the simulations in a test power system. Modelling and simulation of independent random load fluctuations in many loads is numerically challenging and can introduce numerical instability for simulations ranging several minutes. Accordingly, *none of the available commercial transient stability simulation programs can simulate the ambient response of large-scale power system models*. Therefore, we use Kundur test system [22] in this report and the simulations are carried out using Matlab.

Figure 1 shows the single-line diagram of the well-known two-area Kundur system [22] where it is modified to include an SVC at Bus 7. The two-axis representation is used for modeling system generators. Each generator is equipped with a first order AVR and a two-stage PSS to adjust the system damping to the desirable level. SVC operates in voltage regulation mode and is modelled with single order dynamic model, as recommended in manuals available in [24]. The system has a dominant inter-area mode which causes an oscillation of generators 1 and 2 (in Area 1) against generators 3 and 4 (in Area 2) with a frequency around $f = 0.6$ Hz. As an initial setting, the system damping ratio is set to be low at 2% and the ambient data is generated by modulating the system loads (active and reactive load powers at Buses 7 and 9) with white Gaussian noise (1%) around their nominal values and solving the system non-linear equations. We will use five minutes of ambient data to perform the analysis (same as in [18]).

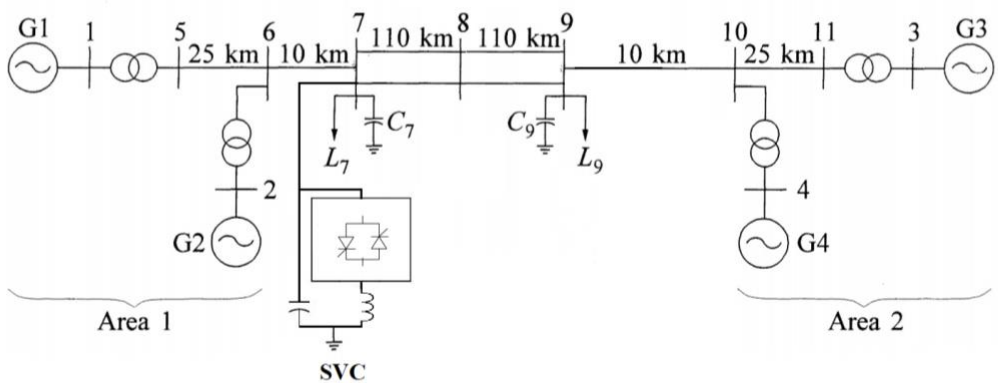

Figure 1. The modified Kundur test system with an SVC at bus 7 [22].

For the feedback we will consider the bus voltage angle differences as feedback signal candidates. As mentioned before, the system inputs are load active and reactive power fluctuations. Accordingly, if the best input is determined as the reactive power injection at a bus, we will need a dynamic VAR-compensator to modulate the reactive power, whereas if the best input is determined as the active power injection at a bus, an energy storage device [25] is needed as the actuator to modulate the active power at the very bus. It may be noted here that a dedicated element is not required for this purpose.

A small portion of the capacity from already installed devices can be reserved for oscillation damping control. This is illustrated later in our control implementation.

3.1 System Identification and Control

In this part, three bus voltage angle differences $y_1 = \delta_5 - \delta_6$ (from Area 1), $y_2 = \delta_{11} - \delta_{10}$ (from Area 2), and $y_3 = \delta_6 - \delta_{10}$ (between Area 1 and Area 2) are considered as feedback signal candidates among which we will choose the best one to use as feedback signal to the feedback controller. These signals will serve as output signals in the identification process. The modulation signals of P_{L7}, P_{L9}, Q_{L7}, and Q_{L9} are system inputs. The three output and four input signals together create twelve channels to be identified. To model the measurement noise, independent white Gaussian noise signals are added to both input signals and output signals (as 1% of amplitude of each signal). Figure 2 shows the estimated transfer functions (magnitude and phase plots) of the twelve channels versus the true ones.

Based on the mentioned channel selection criteria, it can be observed that P-channels have larger residues compared to corresponding Q-channels. This is natural because P-actuation travels longer compared to Q-actuation generally in power systems [22]. However, since active power-based energy storage devices for P-based actuation are not readily available in present-day power systems, we look for a feasible Q-channel with the highest residue. We observe that while the channel (3,4), associated with output $y_3 = \delta_6 - \delta_{10}$ and input Q_{L9}, seems to be the best control channel with reference to our previous discussion, the identified transfer functions indicate the presence of a right half-plane (RHP) zero. That makes it a non-minimum phase channel. All the 100 Monte-Carlo transfer function estimates of this channel show one and only one RHP zero. This is consistent with the presence of a RHP zero at +3.53 in the linearized model-based transfer function. Figure 3 shows the zero estimates from the transfer function estimates from the ambient data for the 100 Monte-Carlo tests of this channel. The mean and standard deviation (STD) of these estimates are 2.875 and 0.432, respectively. These results show the potential use of the proposed approach for identifying the non-minimum phase input-output channels. These channels have the potential to drag the closed-loop system into instability and are thus not preferred from the control theory perspective [10]. In this regard, the channel (3,3) associated with (output $y_3 = \delta_6 - \delta_{10}$ and input Q_{L7}) is chosen as the next best available channel for implementing the feedback control in our example.

An SVC is connected to bus 7 in our modified system. We will use a fraction of SVC VAR-capacity to control inter-area oscillations, more specifically, to improve the damping characteristics of the mode of interest. JCO based queueing of control channels offers online information on the next-in-line best channel in case of unavailability of a resource at a bus or infeasibility of a control channel.

In the next step, we will design the feedback controller for SVC operation, based on the identified transfer function of Channel (3,3). We performed one hundred independent Monte-Carlo simulations, and one hundred transfer functions are estimated for each channel using a five-minute ambient data length with the sampling frequency of 30 Hz. To test the design methodology, we

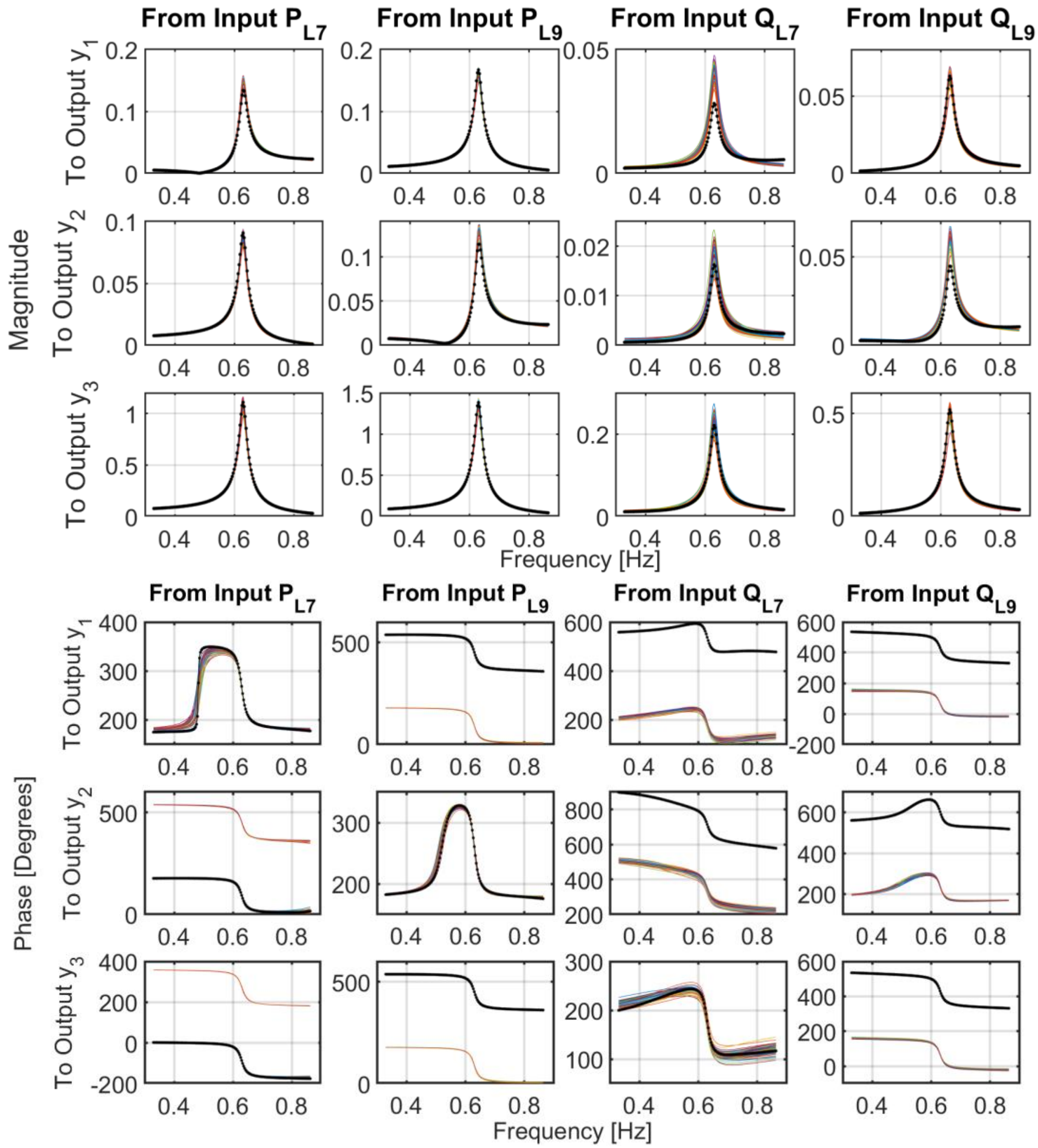

Figure 2. Frequency domain transfer function magnitudes (top) and phase plots (bottom): estimated (colored) versus the true ones (black graphs).

will design the controller based on the worst transfer function estimate (the one with the largest deviation from the true transfer function in the frequency domain). The identified transfer function with the highest deviation from the true transfer function is as follows.

$$G_1 = \frac{-0.01093s^2 - 0.04177s - 0.1829}{s^2 + 0.1594s + 15.71} \tag{7}$$

From the denominator of this identified transfer function, the (open-loop) inter-area mode is at $-0.0797 \pm 3.96i$ and the frequency and the damping ratio of this mode is $f = 0.63\text{Hz}$ and $\zeta = 2.01\%$, respectively. Say we want to increase the mode damping ratio to be above 8%. The designed controller is obtained as follows (A bandpass filter from [26] is added to controller to prevent other modes from getting affected).

$$H_1 = \frac{2s}{s^2 + 2s + 15} \frac{-0.1550\,s - 0.5522}{0.2547\,s + 1} \quad (8)$$

By applying the designed feedback controller to the identified model, the closed-loop system pole is obtained as $-0.366 \pm 4.04i$ which is desirable. As can be seen, the damping ratio of the mode is increased to be above 8%. However, one needs to evaluate the performance of the designed feedback controller on the full system model, rather than the identified model. Table I provides the system modal characteristics from four cases: 1) the actual (linearized) system model without the controller, 2) the identified system model without the controller, 3) the actual (linearized) system model with the controller, and 4) the identified system model with controller. As can be observed, there is a close match between the open- (closed-) loop actual and identified system model quantities indicating that the controller from proposed measurement-based approach has provided enough level of damping for the system. Figure 4 presents the time response, both with and without the designed controller, for the insertion of a 50 MVAR shunt capacitor bank at bus 9 at time t=0 in the modified Kundur system.

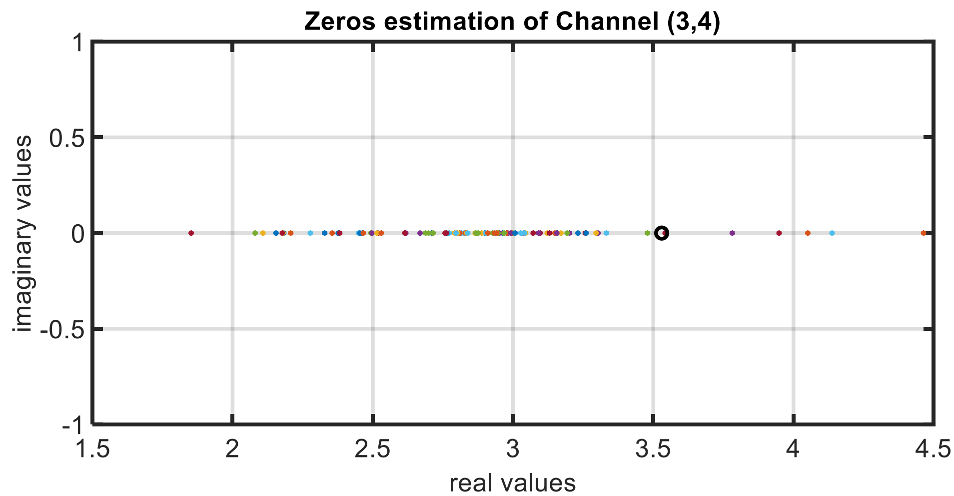

Figure 3. Zeros of channel (3,4): Estimated (colored dots) versus true (large black circle).

Table 1. Estimated versus the true open- and closed-loop system modes.

	Frequency (Hz)	Damping ratio - mean (%)	Damping ratio – STD (%)
Open-loop mode from system linearized model without controller	0.6302	2.02	-
Open-loop mode estimates from ambient data without controller	0.6302	1.98	0.42
Closed-loop mode from system linearized model with controller	0.6350	8.27	-
Closed-loop mode estimates from ambient data with controller	0.6429	8.24	0.45

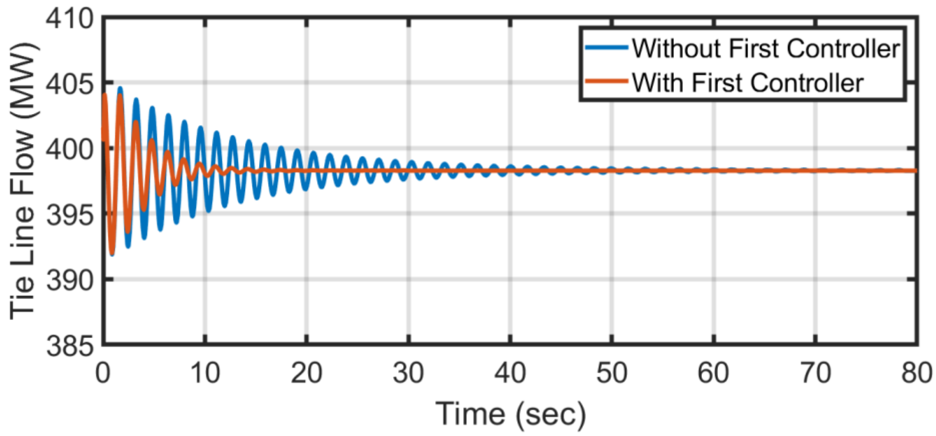

Figure 4. Time response of modified Kundur two-area system for a 50 MVAR shunt capacitor insertion at bus 9 at t=0, demonstrating tie-line oscillation with and without identification-based closed loop control.

To illustrate the adaptive nature of our online ambient data-based control, we simulate a PSS malfunction on generator 1 in area 1, in our closed loop system, specifically we assume that the stabilizer gain changes by accident. If the controller were to remain the same as in (8) (like in offline designs), the damping of the interarea mode would have dropped to 2.30% after the PSS malfunction. However, the controller as proposed identifies the new system transfer function based on ambient data for the closed-loop system that uses the first controller (8) and computes a new set of control parameters which can be implemented as the second outer loop. The identified closed loop transfer function (worst) with PSS malfunction at Bus 1 and the second controller are shown below:

$$\mathrm{G}_2 = \frac{-0.0000856\mathrm{s}^2 - 0.04497\mathrm{s} - 0.06148}{\mathrm{s}^2 + 0.1385\mathrm{s} + 16.19} \tag{9}$$

$$\mathrm{H}_2 = \frac{2\mathrm{s}}{s^2 + 2\mathrm{s} + 15}\frac{-0.1357\,\mathrm{s} - 0.3972}{0.2032\,\mathrm{s} + 1} \tag{10}$$

Table II lists the closed loop characteristics of system with the first controller versus the system with adaptive controller design with the second feedback loop. The adaptive controller keeps up with the changing system conditions leading to a closed loop damping ratio of 8.27%. Figure *5* presents the time response, both with the first controller only and with the adaptive controller in case of PSS malfunction, for the switching of a 50 MVAR shunt capacitor bank at bus 9 in detailed nonlinear dynamic model of the Kundur system.

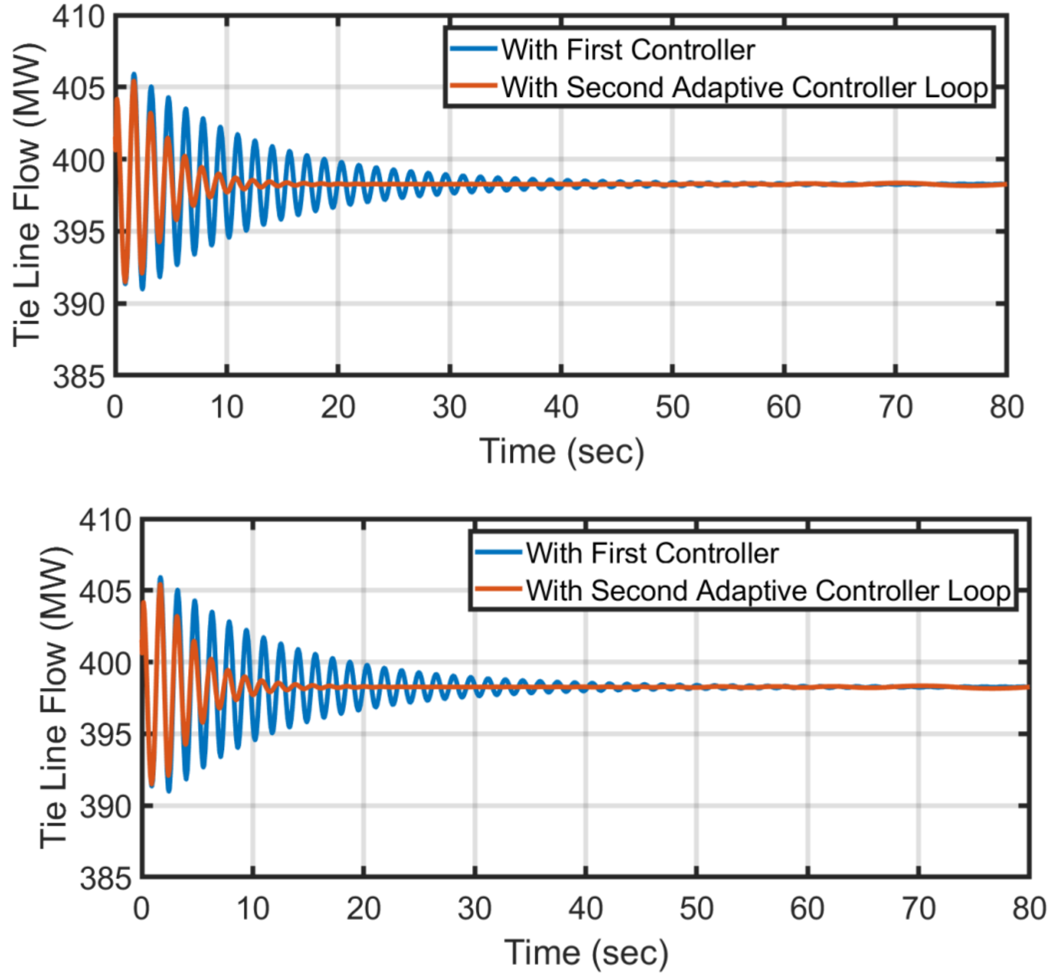

Figure 5. Closed-loop performance comparison of the first vs second adaptive controller loop in case of PSS malfunction on generator 1.

Table 2. Closed-loop system modes with the first and second adaptive controllers after the PSS malfunction.

	Frequency (Hz)	Damping ratio - mean (%)	Damping ratio – STD (%)
Closed-loop mode from system linearized model with the first controller	0.6398	2.02	-
Closed-loop mode estimates from ambient data with the first controller	0.6414	2.00	0.38
Closed-loop mode from system linearized model with the second adaptive controller loop	0.6525	8.08	-
Closed-loop mode estimates from ambient data with the second adaptive controller loop	0.6589	8.26	0.40

This example demonstrates the strength of the model-free damping controller over its offline model-based counterpart. When the system conditions improve, the additional control loop can be removed, and the design can revert back to a single loop design.

3.2 Sensitivity analysis of the proposed identification technique

In this part, first, the sensitivity of the proposed identification method to measurement noise will be examined. To do so, the input-output data obtained in Part A is contaminated with two different levels of white Gaussian multiplicative noise signals (noise with 10% and 50% energy of original noise-free signal) and the identification of the twelve channels is repeated using the same setting. demonstrates the frequency domain transfer function magnitude estimates of the channel (3,3) at the presence of measurement noise. Moreover, the estimate without any measurement noise is also presented for comparison. As can be seen, adding measurement noise has no discernible effect on the accuracy of the identification technique. This is mostly because of simultaneously engaging multiple channels in the identification which have the system poles as a common characteristic. Efficient handling of white measurement noise is also an inherent strength of frequency domain approaches such as the one proposed here.

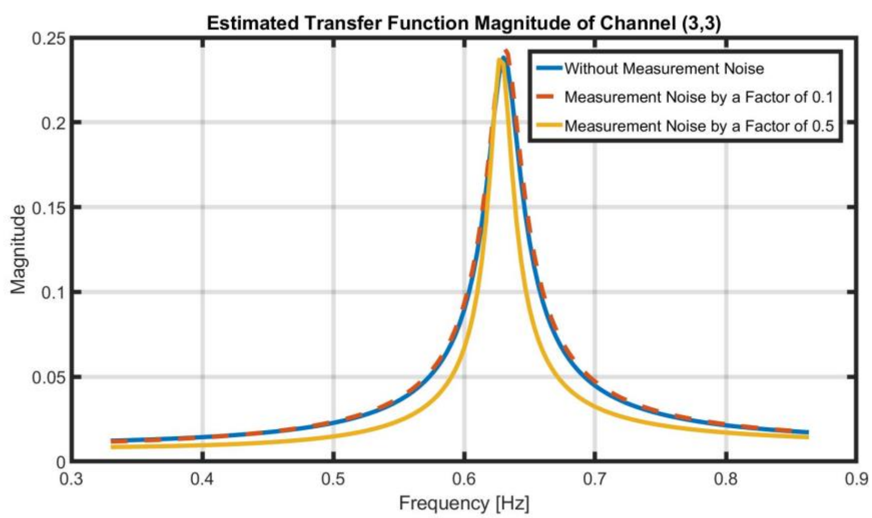

Figure 6. Frequency domain transfer function magnitude estimation with the presence of measurement noise.

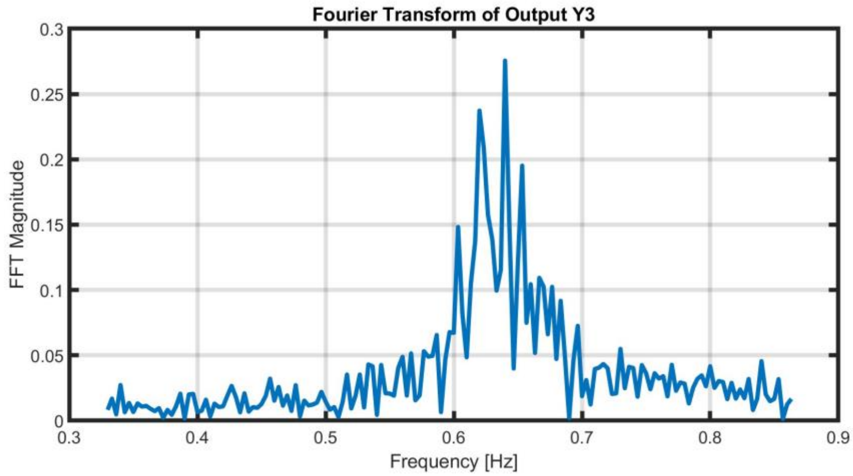

Figure 7. Fourier transform of output y_3 for a sample input signal.

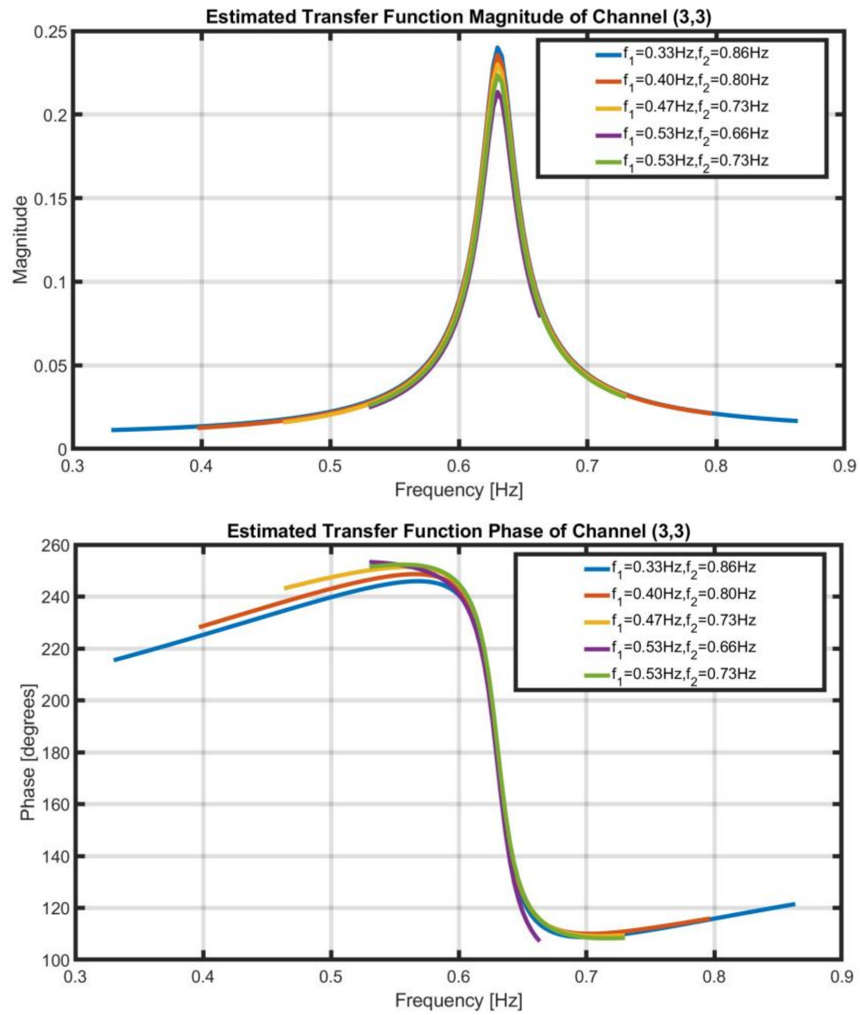

Figure 8. Estimated frequency domain transfer function of channel (3,3): a) magnitude (top), b) phase (bottom).

Next, the sensitivity of the proposed identification method to the selected range of frequency around the mode of interest will be examined. To do so, we will use the same input-output data, but we will choose different ω_1 and ω_2 and perform the identification on the previously mentioned twelve channels. Figure 7 shows the FFT magnitude of Output 3 signal for a sample data. Let us denote the frequency window used in the identification by its corner frequencies, f_1 and f_2.

Figure 8 depicts the estimates of Channel (3,3) frequency domain transfer function for the following f_1 and f_2 choices: 1) $f_1 = 0.33\text{Hz}$, and $f_2 = 0.86\text{Hz}$, 2) $f_1 = 0.40\text{Hz}$, and $f_2 = 0.80\text{Hz}$, 3) $f_1 = 0.47\text{Hz}$, and $f_2 = 0.73\text{Hz}$, 4) $f_1 = 0.53\text{Hz}$, and $f_2 = 0.66\text{Hz}$, and 5) $f_1 = 0.53\text{Hz}$, and $f_2 = 0.73\text{Hz}$. Note that the other eleven identified channels are not shown here for the sake of space. Figure 8 shows that different choices of f_1 and f_2 only have subtle effects on the accuracy of the identification process which in turn indicates the robustness of the proposed identification technique.

3.3 Discussion

The performance features of the proposed framework and the simulations results are discussed below.

1) In the proposed method, the joint controllability-observability of a pair of the input-output channel cannot be determined unless both the input and output signals are measured. For example, if a bus does not have any load to measure or if the load measurements are not available, the JCO of this bus location to system outputs cannot be estimated by the proposed method. Considering the test case above, we will be only able to determine whether the controller should be installed at buses 7 or 9, whereas from the system model-based analysis, bus 8 might be a better control location as shown by some researchers (page 1143, [22]).

2) Those input signals which are exciting the system but are not measured will act as process noise and will impact the estimation of the transfer function of available (measurable) input-output pairs. In other words, the more measurements we have, the better the model estimates we can obtain.

3) In equation (5), the total number of unknowns is $2 + 3\text{NM}$ where 2 corresponds to the denominator parameters σ and Ω and 3NM is from 3 parameters in numerator corresponding to N outputs and M inputs. Now, let us assume that there are n frequency points in the range of $\omega_1 < \omega < \omega_2$. Then, the total number of equations will be 2Nn (Nn from real equations and Nn from imaginary equations). Therefore, as far as the number of frequency points is roughly 1.5 times larger than the number of (dominant) inputs, we will be able to determine the parameters uniquely, in a least-squares sense.

4) As can be seen from the simulation results, the identification method is robust against the measurement noise as it establishes the common properties of all available channels in the identification.

5) The proposed method can point to presence of RHP zeros of channels in the ambient data-estimated transfer functions which can help us avoid the problems associated with non-

minimum phase control designs.

4. Conclusion

In this work, a framework for both identification and adaptive control design of power system low-frequency electromechanical oscillations is proposed. The methodology is entirely based upon PMU ambient measurements and it does not require any knowledge of the system model. As the first step, second-order transfer functions in the Fourier domain are fitted to the measured input-output data in a pre-specified frequency range. Next, the best input-output pair (the controller location and the feedback signal, respectively) for feedback control implementation is determined by choosing the channel with the highest joint controllability-observability. Finally, an appropriate controller is designed by utilizing the identified transfer function and using the Bode plot-based technique. Simulations on a test power system demonstrate the applicability of the proposed framework in identifying and control of a dominant inter-area mode. It is also shown that the proposed identification technique is very robust against the measurement noise. There is only one user specified parameter, namely, the analysis frequency range, and it is shown that it has little effect on the accuracy of estimates. Future work includes examining the applicability of the proposed framework in larger power system models and for wide-area measurements based multiple-input multiple-output (MIMO) control of PSS and modern power electronic controllers for enhanced system stability. Another area of interest could be consideration of communication system issues such as network delays and packet dropouts in the transfer function identification procedure.

References

[1] D. N. Kosterev, C. W. Taylor and W. A. Mittelstadt, "Model validation for the August 10, 1996 WSCC system outage," in IEEE Transactions on Power Systems, vol. 14, no. 3, pp. 967-979, Aug. 1999.

[2] V. Venkatasubramanian, Y. Li, "Analysis of 1996 western American electric blackouts", Proc. Bulk Power System Phenomena-Stability and Control, 2004.

[3] Oscillation Event 03.12.2017, System Proection and Dynamics WG, ENTSOE, available at https://docstore.entsoe.eu/Documents/SOC%20documents/Regional_Groups_Continental_Europe/OSCILLATION_REPORT_SPD.pdf

[4] Eastern Interconnection Oscillation Disturbance, North American Electric Reliability Coordination (NERC): https://www.nerc.com/pa/rrm/ea/Documents/January_11_Oscillation_Event_Report.pdf

[5] J.Pierre, et al., "Identification of electromechanical modes in power systems," IEEE Task Force Report, Special Publication TP462, IEEE Power and Energy Society, July 2012.

[6] G. Liu and V. Venkatasubramanian, "Oscillation monitoring from ambient PMU measurements by Frequency Domain Decomposition," 2008 IEEE International Symposium on Circuits and Systems, Seattle, WA, 2008, pp. 2821-2824.

[7] M. Hatami, M. Farrokhifard and M. Parniani, "A Non-Stationary Analysis of Low-Frequency Electromechanical Oscillations Based on a Refined Margenau-Hill Distribution," in IEEE Transactions on Power Systems, vol. 31, no. 2, pp. 1567-1578, March 2016.

[8] I. Kamwa, R. Grondin and Y. Hebert, "Wide-area measurement based stabilizing control of large power systems-a decentralized/hierarchical approach," in IEEE Transactions on Power Systems, vol. 16, no. 1, pp. 136-153, Feb 2001.

[9] A. Chakrabortty and P. P. Khargonekar, "Introduction to wide-area control of power systems," 2013 American Control Conference, Washington, DC, 2013, pp. 6758-6770.

[10] M. M. Farsangi, Y. H. Song and K. Y. Lee, "Choice of FACTS device control inputs for damping interarea oscillations," in IEEE Transactions on Power Systems, vol. 19, no. 2, pp. 1135-1143, May 2004.

[11] Y. Zhang and A. Bose, "Design of Wide-Area Damping Controllers for Interarea Oscillations," in IEEE Transactions on Power Systems, vol. 23, no. 3, pp. 1136-1143, Aug. 2008.

[12] R. L. Cresap, W. A. Mittelstadt, D. N. Scott and C. W. Taylor, "Operating Experience with Modulation of the Pacific HVDC Intertie," in IEEE Transactions on Power Apparatus and Systems, vol. PAS-97, no. 4, pp. 1053-1059, July 1978.

[13] A. M. A. Hamdan and A. H. Nayfeh, “Measures of modal controllability and observability for first-and second-order linear systems,” AIAA J. Guid. Control Dyn., vol. 12, no. 3, pp. 421–428, 1989.

[14] M. E. Aboul-Ela, A. A. Sallam, J. D. McCalley and A. A. Fouad, "Damping controller design for power system oscillations using global signals," in IEEE Transactions on Power Systems, vol. 11, no. 2, pp. 767-773, May 1996.

[15] Hauer, J.F. 1977. Computer Routines for Fitting Transfer Functions to System Response Measurements. Bonneville Power Administration, Portland, Oregon.

[16] D. J. Trudnowski, Frequency domain transfer function identification using the computer program SYSFIT, Pacific Northwest Lab., Richland, WA, Dec. 1992.

[17] J. R. Smith, F. Fatehi, C. S. Woods, J. F. Hauer and D. J. Trudnowski, "Transfer function identification in power system applications," in IEEE Transactions on Power Systems, vol. 8, no. 3, pp. 1282-1290, Aug. 1993.

[18] H. Liu et al., "ARMAX-Based Transfer Function Model Identification Using Wide-Area Measurement for Adaptive and Coordinated Damping Control," in IEEE Transactions on Smart Grid, vol. 8, no. 3, pp. 1105-1115, May 2017.

[19] P. Van Overschee, B. De Moor, Subspace Identification for Linear Systems, MA, Boston:Kluwer, 1996.

[20] Ning Zhou, J. W. Pierre and J. F. Hauer, "Initial results in power system identification from injected probing signals using a subspace method," in IEEE Transactions on Power Systems, vol. 21, no. 3, pp. 1296-1302, Aug. 2006.

[21] E. C. Levy, "Complex-curve fitting," in IRE Transactions on Automatic Control, vol. AC-4, no. 1, pp. 37-43, May 1959

[22] P. Kundur, Power System Stability and Control. New York, NY, USA: McGrawHill, 1994.

[23] R. C. Dorf, R. H. Bishop, Modern Control Systems, Pearson, 12th edition, 2010.

[24] DSA Tools, Powertech Labs, Canada: https://www.dsatools.com/

[25] J. C. Neely et al., "Damping of inter-area oscillations using energy storage," 2013 IEEE Power & Energy Society General Meeting, Vancouver, BC, Canada, 2013, pp. 1-5, doi: 10.1109/PESMG.2013.6672775.

[26] J. Zhang, C. Y. Chung and Y. Han, "A Novel Modal Decomposition Control and Its Application to PSS Design for Damping Interarea Oscillations in Power Systems," in IEEE Transactions on Power Systems, vol. 27, no. 4, pp. 2015-2025, Nov. 2012.

Part II

Parametric Dependence Analysis and Channel Preserving Model Reduction

Sandip Roy
Subir Sarker, Graduate Student

Washington State University

For information about this project, contact:

Sandip Roy
Professor, School of Electrical Engineering and Computer Science
Washington State University
Email: sandip@wsu.edu

Power Systems Engineering Research Center

The Power Systems Engineering Research Center (PSERC) is a multi-university Center conducting research on challenges facing the electric power industry and educating the next generation of power engineers. More information about PSERC can be found at the Center's website: http://www.pserc.org.

For additional information, contact:

Power Systems Engineering Research Center
Arizona State University
527 Engineering Research Center
Tempe, Arizona 85287-5706
Phone: 480-965-1643

Table of Contents

List of Figures

1. Introduction

1.1 Background

The presence of poorly-damped wide-area oscillations or swings in the bulk power grid is often an indicator of system inefficiency, and a harbinger of costly system-wide failures [1]. New wide-area control technologies being deployed in the grid, including modulation schemes for High Voltage Direct Current (HVDC) lines and new Flexible AC Transmission System (FACTS) controllers, hold great promise to alleviate undesirable oscillations and hence reduce the frequency of system-wide failures [1], [2]. However, the design and coordination of wide-area control systems to damp oscillations remains a challenging problem, for several reasons: 1) increasing variability in operating conditions of the grid, which influence the swing dynamics; 2) a lack of understanding of control-channel properties in the analysis of the swing dynamics, which has traditionally focused on modal (intrinsic) properties or exhaustive simulation; 3) difficulty of designing multi-faceted controls which are often managed by multiple authorities [3] –[6].

1.2 Relevant Literature

Motivated by the broad aim of assessing and designing wide-area controls for the power grid, there has been a recent effort in the controls-engineering community to characterize the swing-dynamics of the grid from an input-output or transfer-function perspective [7] –[11]. These various studies primarily focus on the classical model for the swing dynamics, which tracks electrical frequencies and angles at network buses using an inertial (mass-spring-type) model. One thrust in this effort has been to characterize transfer-function zeros, and in particular the presence/absence of nonminimum-phase zeros, from a topological standpoint; these characterizations of zeros allow identification of channels that are amenable for or difficult to control, and ones that may susceptible to undesirable disturbance responses. A second thrust has been focused on metrics for input-output performance, which may be defined from the frequency response or time-domain constructs (e.g. Gramians).

1.3 Focus of this Effort

This study continues the input-output analysis of the power grid's swing dynamics [9], [10], focusing on the challenge that grid operating conditions are highly variable in networks with high renewables penetration [4]. Specifically, to allow evaluation of channel properties across variable operating conditions, we examine how the zeros of input-output channels in the classical swing-dynamics model depend on operating parameters of the network, including bus inertias and damping, and effective line susceptances. The influence of these parameters on the presence or absence of nonminimum-phase zeros is determined from a graph-theoretic standpoint, and some bounds on network parameters guaranteeing minimum-phase dynamics are also developed. The implications of the results with regard to wide-area control of the power grid are discussed, and several examples are presented to illustrate the results. In this regard, we specifically draw on the graph-theoretic analysis to understand model reduction for controller design – we illustrate that reduced models obtained via standard reduction techniques may be problematic, and

While the study described here is concerned specifically with the classical swing-dynamics model, it is part of a broader effort to characterize input-output properties of canonical dynamical-network models [12] –[16]. In particular, parallel input-output analyses have also been undertaken for models of distributed consensus, infectious-disease spread, and coupled-oscillator synchronization [5], [17] –[25]. Within this broader context, this study explores how model parameters influence channel phase characteristics in such network models, and also introduces approaches for finding bounds on parameters that guarantee minimum-phase channel dynamics. Methodologically, our analysis exploits structural representations of linear-system input-output dynamics together with graph-theory and nonnegative-matrix constructs; many of these methods carry through to the other network models considered in the literature.

1.4 Report Organization

The rest of the report organized as follows. In Section 2, the input-output swing-dynamics model is reviewed. In Section 3, several structural and graph-theoretic results on the zeros of the nominal swing-dynamics model are given, focusing on how zero structures depend on model parameters. Several examples are presented to illustrate the results, and give an indication of parameter thresholds that distinguish minimum-phase and non-minimum-phase behaviors (Section 4). Implications on model reduction are presented in Section 5. Finally, proofs of the formal results are included as an appendix.

2. Modeling

Input-output characteristics of the bulk power grid's swing dynamics are considered, in the context of the linearized classical model for the swing dynamics.

The electromechanical dynamics of the synchronous power network are known as the swing dynamics. In this study, we consider the classical model for the swing dynamics, which is a nonlinear differential-algebraic equation (DAE) model that tracks electrical angles and frequencies at network buses, and represents synchronous generators as inertial elements. Following on the standard techniques in power-system dynamic analysis, we consider a reduced purely-differential model for the swing dynamics, wherein the algebraic equations for the passive (load-only) buses have been solved out [27], [28]. Also following on the formal analysis of the swing dynamics, we focus on the linearization of the the reduced swing dynamics model.
To enable assessment of input-output properties, a single-input single-output channel is imposed on the linearized swing-dynamics model, where the input is abstractly modeled as a power injection/extraction at a single bus, and the output is a frequency or angle measurement at a single (possibly different) active bus (see also [9], [10]); channels models of this form are represent a wide-area control channel of interest, or a disturbance response of concerns.

Formally, for a power transmission network with n synchronous generators, the linearized reduced swing dynamics model with input-output channel is the following:

$$\begin{bmatrix} \dot{\delta} \\ \dot{\omega} \end{bmatrix} = \begin{bmatrix} 0 & I \\ -H^{-1}L(\Gamma) & -H^{-1}D \end{bmatrix} \begin{bmatrix} \delta \\ \omega \end{bmatrix} + \begin{bmatrix} 0 \\ \mathbf{e}_i \end{bmatrix} u \qquad (1)$$

$$y = \begin{bmatrix} 0 & \mathbf{e}_j^T \end{bmatrix} \begin{bmatrix} \delta \\ \omega \end{bmatrix}$$

where $\delta(t) = \begin{bmatrix} \delta_1 & \cdots & \delta_n \end{bmatrix}^T$ represents the electrical angles at the n buses at time t (relative to a nominal trajectory), $\omega(t) = \begin{bmatrix} \omega_1 & \cdots & \omega_n \end{bmatrix}^T$ represents the electrical frequencies at the buses, the notation $\mathbf{e}_q$ represents a 0-1 indicator vector with qth entry equal to 1, the scalar input $u(t)$ is a power-injection signal at bus i, and the scalar output $y(t)$ is the frequency at bus j. The model is defined by the following parameters: the positive diagonal matrix H represents the rotational inertias of the generators at the buses, the positive diagonal matrix D captures the frequency dampings of the generators, and the matrix $L(\Gamma)$ is a symmetric positive semidefinite matrix (under the standard assumption that the transfer conductances in reduced network are negligible) that entirely specifies the dynamic interactions among the buses in reduced network.
We specify the matrix $L(\Gamma)$ in terms of a graph Γ, so as to enable a graph-theoretic analysis of the dynamics. Γ is defined to be an undirected weighted graph whose vertices represent the active buses (buses with inertial generation). Each off-diagonal entry of the matrix $L(\Gamma)$ equals the negative of the edge weight between the corresponding vertices in the graph Γ if there is an edge, and equals zero otherwise. The diagonal entries of $L(\Gamma)$ are positive, and at least as large as the absolute sum of the off-diagonal entries on the corresponding row or column. We assume throughout the article that Γ is connected. We refer to the graph Γ as the network graph. Also, the nodes in the network where the input is applied and the output is measured (i and j, respectively) are referred to as the input and output nodes, and the corresponding vertices in the graph are referred to the the input and output vertices. We note that the edge weights in the network graph

can be interpreted as equivalent effective susceptances between buses at the operating point, upon reduction of the passive buses.

The simplified model for the swing dynamics considered here is widely used in the power-engineering community [27]–[30], and also can be viewed a linearization of nonlinear Kuramoto oscillator-type model for the swing dynamics that has been of interest to controls engineers [7]. However, we stress that the model has been enhanced to explicitly represent an input-output channel, in contrast with most of the literature which focuses on internal or modal characteristics. The model is apt for our studies, since it captures the essential oscillatory dynamics of the synchronous generators in the grid, which primarily impact the control and disturbance response of the system.
It can easily be checked all eigenvalues of state matrix

$$\begin{bmatrix} 0 & I \\ -H^{-1}L(\Gamma) & -H^{-1}D \end{bmatrix}$$

are in the open-left half plan (OLHP), except that there may be one eigenvalue at the origin in the special case that generator effective shunt susceptances are negligible in the reduced network. In this case, $L(\Gamma)$ is a Laplacian matrix, and hence $L(\Gamma)$ and in turn the state matrix have a zero eigenvalue.

3. Dependence of the Zero Structure on Network Parameters

The main purpose of this section is to develop structural and graph-theoretic characterizations of the input-output swing-dynamics model, with a focus on understanding how system parameters influence the zero structure of the channel model. In previous works [9], [10], we developed the algebraic machinery that enables structural and graph-theoretic characterization of the zeros. Furthermore, we developed several basic graph-theoretic conditions for minimumphase input-output dynamics. It was shown that the dynamics are minimum-phase if: 1) the input and output are collocated, 2) there is a single path between the input and output in the network graph, 3) the shortest input-output path is sufficiently strong compared to alternative paths, or 4) the generators have high damping.

Here we extend the input-output analysis of the swing dynamics, with the aim of understanding the dependence of input-output characteristics, particularly zero locations, on the generation and network parameters of the model (Section III). The analyses are important for understanding how variations in system operating points and inertias, which are becoming increasingly common with high penetration of intermittent renewables, influence a channel transfer function. They are also a starting point understanding how deployed or planned control systems influence the power grid's dynamics. Specifically, several conditions for minimum-phase or nonminimum phase dynamics are presented for the input-output swing-dynamics model. These results show how the phase characteristic depends on model parameters including inertias, graph edge weights, and damping. In each of these results, we consider the impact of changing a single parameter on the presence/absence of nonmimum-phase dynamics.

The first two theorems indicate circumstances where generators with high damping or high inertia may cause a remote control channel to become nonminimum phase (i.e., to have right half plane zeros). These conditions are important because they identify situations where changes in operating conditions or deliberate design choices may yield nonminimum-phase behaviors. Generally, increases in damping and inertia are assumed to improve stability properties of the power grid, but the theorems show that such increases can actually make particular channels susceptible to oscillations in the sense that they are nonminimum phase. The theorems require some further notation. First, we use the notation d_{ij} for the distance between the input and output vertices *i* and *j* in graph Γ, defined as the minimum number of directed arcs from the vertex *i* to vertex *j*. Also, we refer to a path from the input *i* to the output *j* of minimum length as a *special input-output path*. Similarly, we use the notation $d_{ij}^{(r)}$ for the length of a minimum length path between vertices *i* and *j* which does not pass through vertex *r*. Now we present the theorems:

Theorem 1: Consider the input-output swing-dynamics model (1). In the network graph Γ, suppose that vertex *r* is remote from the input and output vertices *i* and *j* (i.e. $r \neq i,j$), and further $d_{ij}^{(r)} \geq d_{ij} + 2$. If the inertia H_r (i.e. the inertia of the generator corresponding to vertex *r*) is sufficiently large, the input-output swing-dynamics model (1) has some zeros in open right half plane (ORHP).

Theorem 2: Consider the input-output swing-dynamics model (1). In the network graph Γ, suppose that vertex *r* is remote from the input and output vertices (i.e. $r \neq i,j$) and $d_{ij}^{(r)} \geq d_{ij} + 1$. If the damping

D_r (i.e. the damping of the generator corresponding to vertex *r*) is sufficiently large, the input-output swing-dynamics model (1) has some zeros in open right half plane (ORHP).
The theorems 1 and 2 show that a generator with high inertia or high damping necessarily incurs nonminimumphase dynamics, if its corresponding graph vertex disrupts the shortest input-output path of the channel of interest.

Remark: In our previous work [10], we showed that the zeros of the input-output swing-dynamics model (1) do not depend on the damping and inertia of the generators at the input and output locations in graph Γ; the above results show that damping and inertia at remote locations do have an impact.

Similarly, in case that the matrix L is a grounded Laplacian (which corresponds to non-negligible effective shunt susceptances in the network), the following theorem shows that increasing the diagonal entries of the matrix L might incur nonminimum-phase dynamics. The diagonal entries of the matrix L become larger as the effective shunt susceptance (i.e. the effective susceptance between an active bus and the reference generator bus) is increased. Thus, increased diagonal entries should correlate with more stable dynamics; however, again it is seen that such increases may create nonminimum-phase dynamics.

Theorem 3: Consider the input-output swing-dynamics model (1). In the network graph Γ, suppose that vertex *r* is remote from the input and output vertices (i.e. $r /= i,j$), and further $d_{ij}^{(r)} \geq d_{ij} + 1$.

If the diagonal entry L_{rr} of the Laplacian matrix is sufficiently large, the input-output swing-dynamics model (1) has some zeros in the open right half plane (ORHP).
In contrast to the above results, the following theorems give conditions under which generators with high damping or high inertia at some buses can be used to achieve minimum-phase dynamics for a channel of interest. These results require some further terminology regarding the network input-output model. As defined before, the notation d_{ij} is used for the length of the special input-output path, i.e. for the distance between the input vertex *i* and output vertex *j*. Additionally, we define a modified system based on a subgraph of Γ. Specifically, we consider the nominal input-output swing-dynamics model, with a subset of vertices deleted. Consider the input-output swing-dynamics model (1) for an arbitrary graph Γ. Formally, let us consider a subset of vertices $V \subset \{1,\ldots,n\}$, which does not include the input and output vertices (*i* and *j*). Considering a general vector $\mathbf{z}$ with *n* entries, let us define the vector $\mathbf{z}^{(V)}$ as a modified version of the vector $\mathbf{z}$, where the entries $i \in V$ are omitted. Similarly, considering a general matrix A with dimension (n,n), $A^{(V)}$ is a submatrix of A obtained by deleting the rows and columns specified in V. Then, the deletion subsystem is defined as:

$$\begin{bmatrix} \dot{\delta}^{(V)} \\ \dot{\omega}^{(V)} \end{bmatrix} = \begin{bmatrix} 0 & I \\ -H^{-1^{(V)}} L(\Gamma)^{(V)} & -H^{-1^{(V)}} D^{(V)} \end{bmatrix} \begin{bmatrix} \delta^{(V)} \\ \omega^{(V)} \end{bmatrix} + \begin{bmatrix} 0 \\ \mathbf{e}_i^{(V)} \end{bmatrix} u$$
$$y = \begin{bmatrix} 0 & \mathbf{e}_j^{T^{(V)}} \end{bmatrix} \begin{bmatrix} \delta^{(V)} \\ \omega^{(V)} \end{bmatrix} \quad (2)$$

The deletion system (2) is associated with a weighted deletion graph $\Gamma^{(V)}$, which is the induced subgraph of Γ obtained upon omission of the vertices in V from the graph Γ. Also we define $d_{ij}^{(V)}$ as the distance between the input and output vertices (i.e. from vertex *i* to *j*) in graph $\Gamma^{(V)}$.

Now, we present the theorems that show how generators with high damping or inertia placed at some special locations in the network can move zeros of the nominal input-output swing dynamics model (1) to the left half plane.

Theorem 4: Consider the input-output swing dynamics model (1). In the network graph Γ, suppose that vertex r is remote from the input and output vertices (i.e. $r \neq i,j$), and further $d_{ir} + d_{rj} > d_{ij}^{(r)}$. If the inertia H_r (i.e. the inertia of the generator corresponding to vertex r) is made sufficiently large, the input-output swing-dynamics model (1) has zeros that are arbitrarily close to the zeros of the deletion system (2) for $V = \{r\}$ and two zeros arbitrary close to $s = 0$, while all other zeros are in the OLHP.

Theorem 5: Consider the input-output swing dynamics model (1). In network graph Γ, suppose that vertex r is remote from the input and output vertices (i.e. $r \neq i,j$), and $d_{ir} + d_{rj} > d_{ij}^{(r)}$. For sufficiently large damping D_r (i.e. the damping of the generator corresponding to vertex r), the input-output swing-dynamics model (1) has zeros that are arbitrarily close to the zeros of the modified system (2) for $V = \{r\}$ and one zero arbitrary close to $s = 0$, while all other zeros are in the OLHP.

The above theorems demonstrate that increased inertia or damping away from the special input-output path can in some cases promote minimum-phase dynamics, if the modified vertex (bus) is away from the special input-output path. Specifically, in these cases, the zeros reduce to the zeros of the deletion subsystem with the modified vertex removed. Thus, if the removal of this vertex alters the graph in such a way that minimum-phase dynamics are guaranteed, then minimum-phase behavior is also expected in the original system. For instance, if the deletion graph is a tree, then the channel is guaranteed to be minimum phase. The result generalizes to the case where dampings or inertias are augmented at multiple vertices. This indicates the possibility of deliberately designing or verifying generator parameters (typically dampings) at a small set of buses to ensure channels of interest are minimum phase.

Remark: Formally, the channel transfer function can only be weakly minimum phase, since the input-output model will always have a zero at the origin. The zero at the origin reflects that the output is an electrical frequency rather than an angle, and hence a feedback control will be not eliminate offsets in the angle; such offsets are however not detrimental to the function of the grid, and hence a weakly minimum-phase channel is adequate and desirable in this setting.

Next we present some inequality conditions or bounds on the network parameters, which guarantee that the input-output dynamics are weakly minimum phase (i.e., the model has one zero at $s = 0$ and other zeros are in the OLHP). These conditions are important since they provide a quantitative test for ensuring minimumphase dynamics on a channel. Of note, they are valid even if the network graph is directed (the L matrix is asymmetric).

Theorem 6: Consider the input-output swing dynamics model (1) for an arbitrary graph Γ. Suppose that the input vertex *i* and the output vertex *j* are adjacent in network graph Γ. The input-output swing-dynamics model (1) has all zeros in the OLHP except one zero at $s = 0$ if for $\forall k \neq i,j$:

$$2\,|L_{kk}| + 2\left|\frac{L_{jk}L_{ki}}{L_{ji}}\right| \geq \sum_{m\neq i,j} \frac{D_m + H_m}{D_m}\left|L_{km} - \frac{L_{ki}L_{jm}}{L_{ji}}\right|$$

$$D_k \geq \sum_{m\neq i,j} \frac{D_m + H_m}{D_m}\left|L_{km} - \frac{L_{ki}L_{jm}}{L_{ji}}\right|$$

Theorem 7: Consider the zeros of the input-output swing dynamics model, and assume that input vertex and output vertex are the same as vertex *i* in network graph Γ. The input-output swing-dynamics model (1) has all zeros in the OLHP except one zero at $s = 0$ if for $\forall k \neq i$:

$$2\,|L_{kk}| \geq \sum_{m\neq i} \frac{D_m + H_m}{D_m}\,|L_{km}|$$

$$D_k \geq \sum_{m\neq i} \frac{D_m + H_m}{D_m}\,|L_{km}|$$

The previous two theorems provide sufficient conditions for a channel of interest to be minimum phase. For example, the theorems show that by increasing the damping of all generators over certain limits, a channel of interest can be made minimum phase.

4. Example

A small-scale example with six buses is used to illustrate the results on transmission networks (Fig. 1). The channel of interest comprises an input at bus 1 and output at bus 3. The generator at each bus has inertia $h = 1$ and damping $d = 0.2$, and the edge weights (effective line susceptances) are shown in the figure and are all equal to 1. Out goal is to study the effect of a generator's damping and inertia on the zero location.

Based on theorem 2, the input-output model should have RHP zeros if the damping of generator 2 is increased. This is verified in Fig. 2. Similarly, based on theorem 1, if the inertia of generator 2 is sufficiently increased, the input-output model should have RHP zeros. This is verified in Fig. 3.

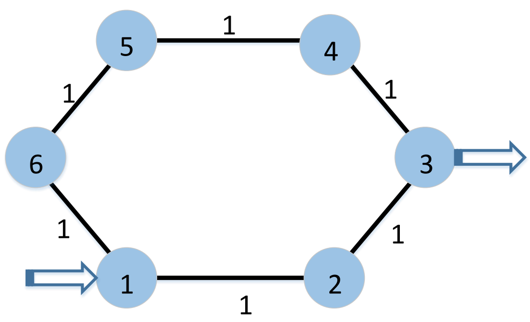

Figure 1: A 6-bus example is developed to gain further insight into the dependence of zeros on generator's parameters

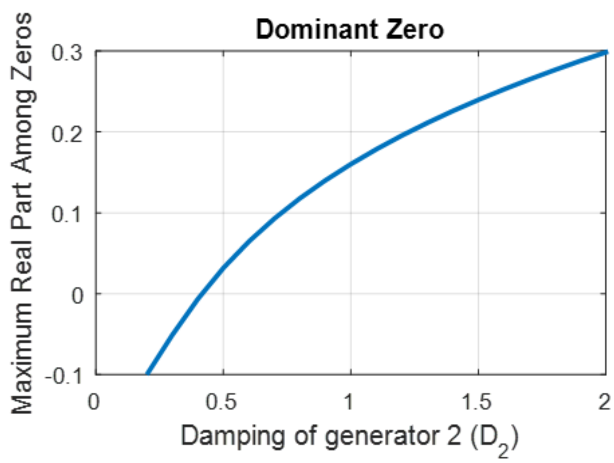

Figure 2: The dependence of the dominant zero location (the largest real part among the zeros) on the damping of the generator 2.

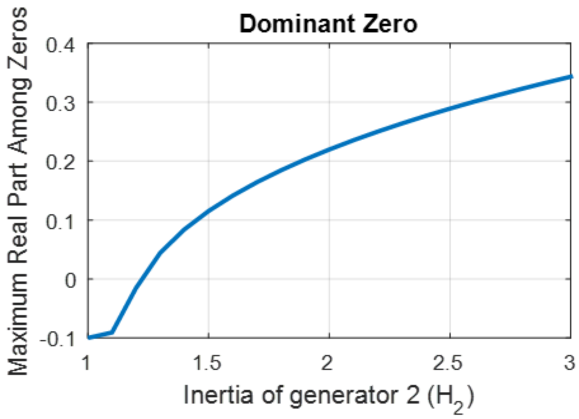

Figure 3: The dependence of the dominant zero location (the largest real part among the zeros) on the inertia of the generator 2.

5. Model Reduction to Preserve Zero Structure: Example and Overview

The above analyses of the swing dynamics model illustrate that the zeros exhibit a sophisticated dependence on the parameters and the graph structure of the network model. This sophisticated dependence suggests that procedures for reducing the dimension or complexity for power system models, which are commonly used in assessing the swing dynamics of the models, may modify the zero structure of a network model. We illustrate in this section that the modification of the zero structure when standard model reduction techniques are used, while hidden in simulations of the native dynamics of the power grid, can lead to substantially altered predictions when controls are used within the power grid. These mis-predictions suggest that reduced models should be used with care in the scope of control design. Based on the illustrative example and the prior-developed results, we briefly propose an alternate model-reduction strategy that can also preserve the zero structure.

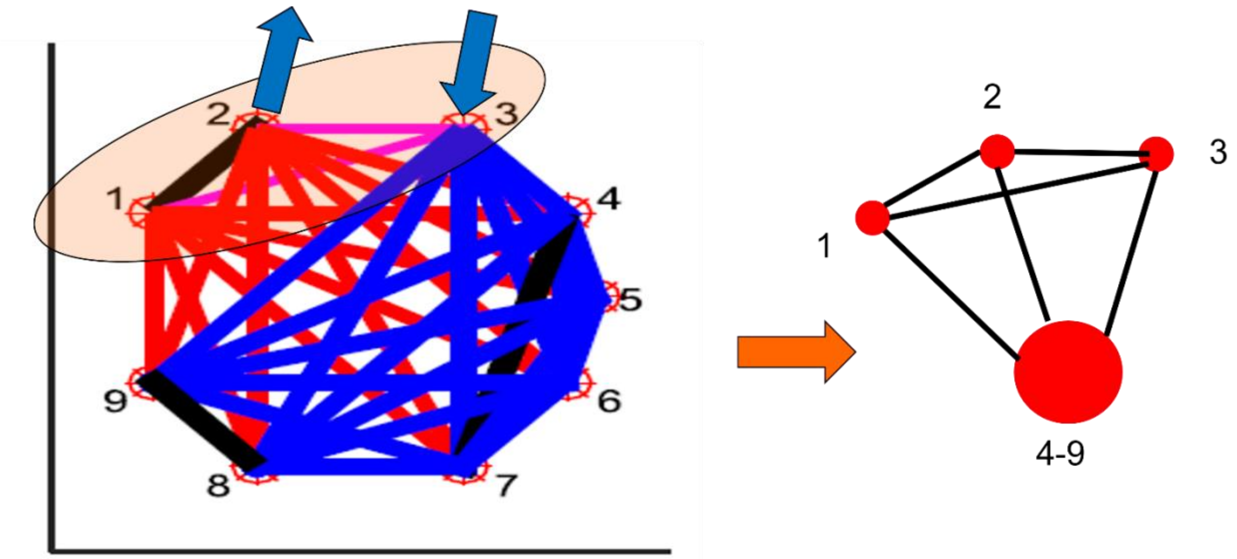

Figure 4: The linear differential-equation model, drawn from a wind-farm planning model for Northwest France, is shown. The goal of the model reduction, which aims to condense 6 of the onshore generator buses, is also illustrated.

The development in this section focuses entirely on a small-scale example model, illustrated in Figure 4. The example, which is an abstraction of a model used for off-shore wind-farm planning in Northwest France, comprises 64 buses which include 9 buses with generation. Two generator buses (1 and 2) are off-shore, and have substantial wind generation with low inertia. The remaining seven generator buses (3-9) are onshore, and are associated with high-inertia spinning generation (specifically, nuclear power plants). The linearized differential-algebraic-equation model for the network has been obtained, and further the algebraic equations have been solved out to obtain a differential equation model with states corresponding to the generator buses; effective line susceptances in the linearized differential-equation model are shown in Figure 4. We are interested in developing a reduced model, which condenses Buses 4-9 to a single bus. We would like to use the reduced model to simulate the dynamics at Buses 1-3, and also to evaluate a control that is applied between buses 2 and 3 (i.e., which uses data from bus 3 to set an input at bus 2).

A standard model reduction technique – specifically a coherency-based reduction-- has been applied to the example. The model is seen to preserve well three fast modes associated with the preserved area, at 1, 1.8, and 2.4 Hz. A single global slow mode is also preserved. Figure 5 shows that the response at Bus 3 due to an impulse input at Bus 2 is very well preserved by the reduced model, as would be expected when the modal dynamics are accurately preserved.

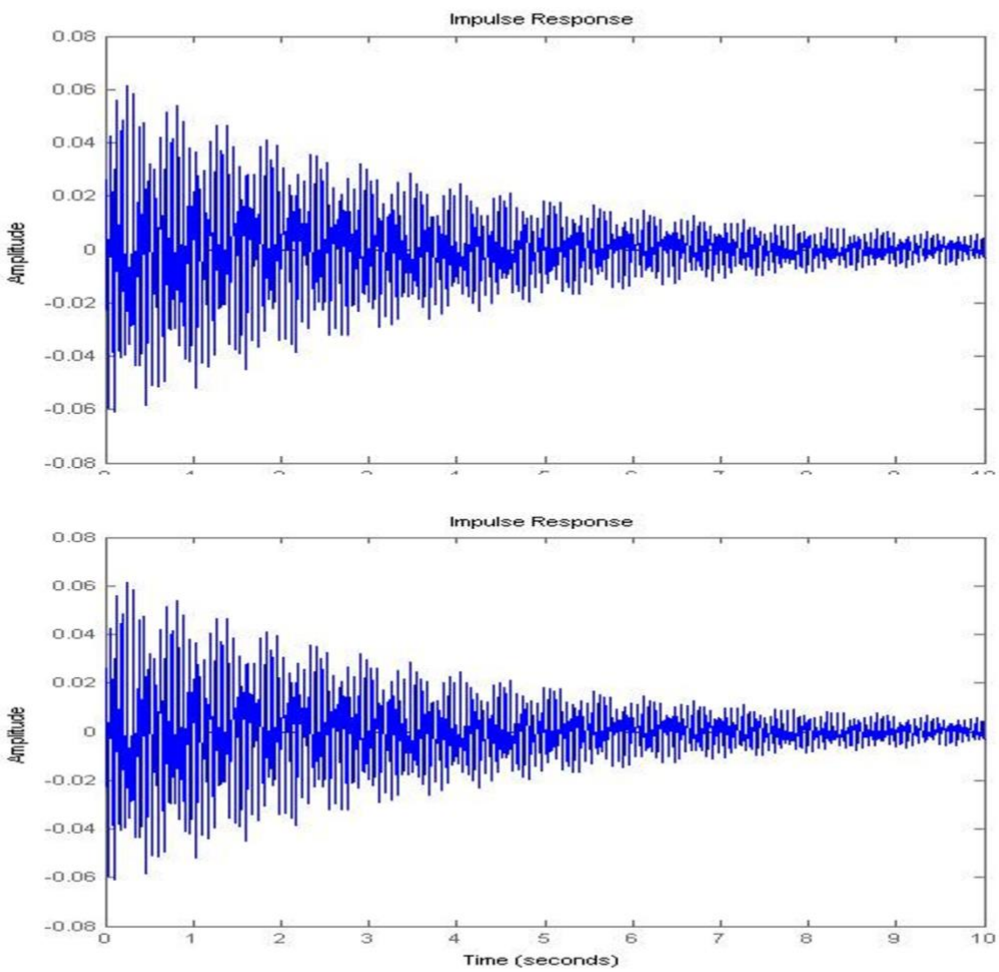

Figure 5: The impulse responses of the original (top) and reduced (bottom) models are almost identical.

However, an analysis of the channel from bus 2 to bus 3 indicates that the model-reduction is not able to preserve input-output properties of the channel, even though the channel is entirely within the preserved region. In particular, the channel in the reduced model is seen to be minimum phase, even the channel is nonminimum phase in the original model. This changed characteristic is also apparent in the frequency response of the model (Figure 6). The two models have nearly identical phase characteristics, indicating that the impulse response of the models should be similar, but they show a different phase characteristic at high frequencies reflecting the change from a nonminimum phase to a minimum phase model. A main consequence of the changed channel property is that the response of the network to a high-gain control on the channel of interest is mis-predicted. Specifically, a large gain causes the original model to become unstable, while appearing to maintain stability in the reduced model (Figure 7).

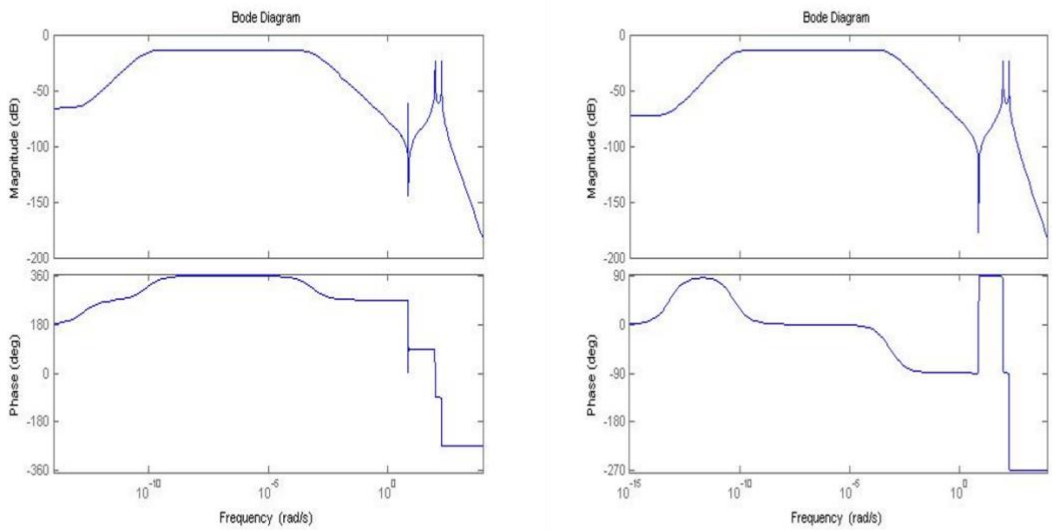

Figure 6: The frequency responses of the original (left) and reduced (right) models are shown. The Bode magnitude plots are amost identical, but the Bode phase plots differ at high frequency, reflecting the fact that the reduced model is a minimum phase system while the original model is not.

The example suggests that coherency-based reduction may be problematic, when the reduced model is used for control system analysis and design. Although we do not demonstrate it here, we have also developed examples which show that balanced truncation-based model reduction approaches suffer from similar concerns.

Given these limitations, it is of interest to develop new model reduction strategies which are able to preserve zero structures on critical channels, in addition to modal and energy properties within a region of interest. We have developed a new model-reduction approach which: 1) preserves a region of interest within the network's graph while condensing other portions of the network (like coherency-based methods), 2) continues to approximate modal behaviors in the critical area, and 3) preserves input-output properties for some critical channels within the region of interest. This new *graph feedback approach* depends on two main insights. First, the approach preserves a larger portion of the network than the region of the interest, which we call the critical area, in a way that zero properties of critical channels within the region of interest are also guaranteed to be preserved; this is done by using the graph-theoretic results about zeros developed above, which give criteria on the network graph such that key zero properties (e.g., nonminimum-phase dynamics) are preserved. Second, the approach recognizes that the remainder of the network outside of the critical area (say, the non-critical area) can be represented as a feedback interconnection with the critical area, whereupon a standard model-reduction technique like balanced truncation can be used for this area. The approach is diagrammed in Figure 8.

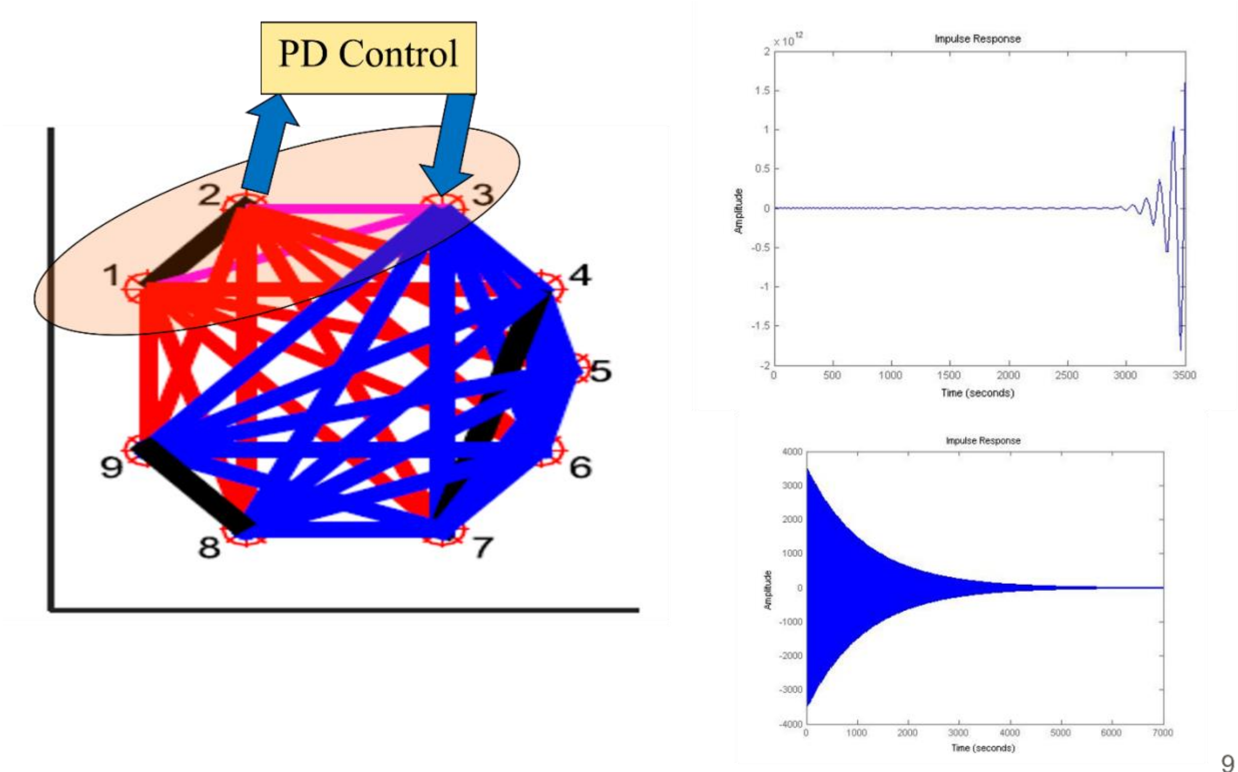

Figure 7: The reduced model is not able to predict the behavior of the original when a high-gain feedback controller is applied at the critical channel, since the nonminimum phase dynamics is no longer present.

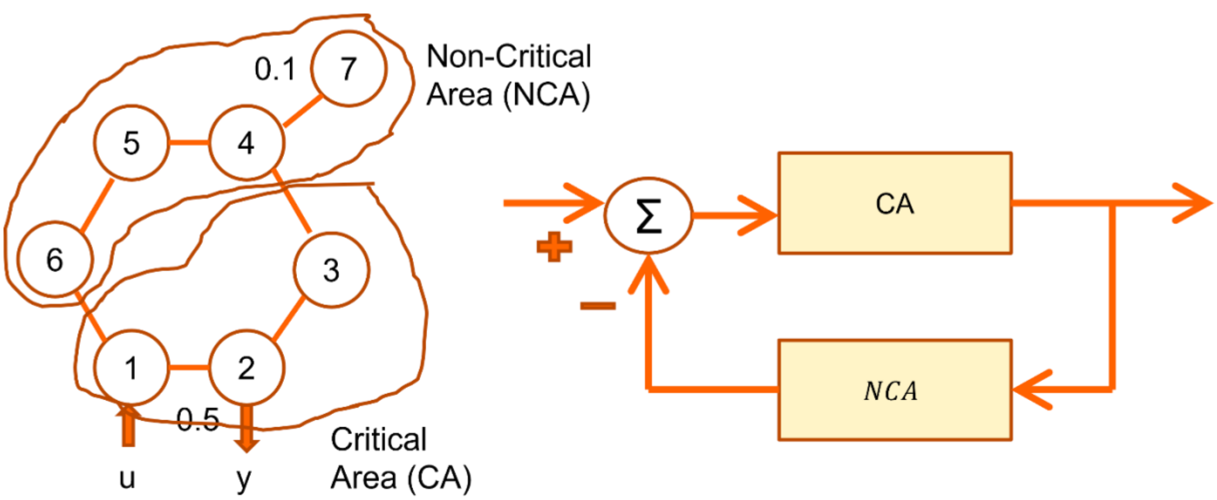

Figure 8: The graph-feedback approach to zero-preserving model reduction is illustrated in a cartoon form.

Appendix

Proof of Theorem 1: Consider V_r as the set of all numbers from set $\{1,2,\ldots,n\}$ except the number r. The network input-output swing-dynamics model (1) can be represented as an interconnection of the following two subsystems C_1 and C_2 (see Fig. 4):

Subsystem C_1, which has two inputs (i.e. u and u_1) and two outputs (i.e. y and y_1), is governed by:

$$\begin{bmatrix} \dot{\bar{\delta}} \\ \dot{\bar{\omega}} \end{bmatrix} = \begin{bmatrix} 0 & I \\ -\bar{H}^{-1}\bar{L}(\Gamma) & -\bar{H}^{-1}\bar{D} \end{bmatrix} \begin{bmatrix} \bar{\delta} \\ \bar{\omega} \end{bmatrix} + + \begin{bmatrix} 0 \\ \bar{\mathbf{e}}_i \end{bmatrix} u + \begin{bmatrix} 0 \\ -\bar{H}^{-1}\bar{L}_{:,r} \end{bmatrix} u_1$$

$$y_1 = \begin{bmatrix} \bar{L}_{r,:} & 0 \end{bmatrix} \begin{bmatrix} \bar{\delta} \\ \bar{\omega} \end{bmatrix}$$

$$y = \begin{bmatrix} 0 & \bar{\mathbf{e}}_j^T \end{bmatrix} \begin{bmatrix} \bar{\delta} \\ \bar{\omega} \end{bmatrix} \qquad (3)$$

where $L_{:,r}$ is the rth column of the matrix L, $L_{r,:}$ is the rth row of the matrix L, and also considering general variable O for using smaller notation, operator $\bar{O}$ stands for $O^{(Vr)}$ which is defined after theorem 3. Subsystem C_2 is governed by:

$$H_r\, \delta r'' + D_r\, \delta r' + L_{r,r}\, \delta r = u_2 \qquad (4)$$

$$Y_2 = \delta r$$

The subsystems together are equivalent to the network input-output model (1) when they are interconnected as follows: the output y_1 of subsystem C_1 is fed into the input of u_2 of subsystem C_2, and the output y_2 of the subsystem C_2 is fed into the input u_1 of subsystem C_1 (see Fig. 4).

We find it convenient to define the following transfer functions from the two subsystems individually. From subsystem C_2 (4), we define the transfer function

$$T_5(s) = \frac{Y_2(s)}{U_2(s)} = \frac{1}{H_r s^2 + D_r s + L_{r,r}}.$$

Similarly, from sub-system C_1 (3), we define the transfer functions $T_1(s) = \frac{Y_1(s)}{U(s)}$, $T_2(s) = \frac{Y(s)}{U_1(s)}$, $T_3(s) = \frac{Y(s)}{U(s)}$, and $T_4(s) = \frac{Y_1(s)}{U_1(s)}$.

(We note here that $T_3(s)$ is distinct from the transfer function for the full network input-output model, since the subsystem C_1 is being considered in isolation in this case.

From the block diagram, it is easy to show that:

$$\begin{aligned} T(s) &= \frac{Y(s)}{U(s)} \\ &= T_3(s) + \frac{T_1(s)T_5(s)T_2(s)}{1 - T_5(s)T_4(s)} \\ &= \frac{T_3(s) + T_5(s)[T_1(s)T_2(s) - T_3(s)T_4(s)]}{1 - T_5(s)T_4(s)} \end{aligned}$$

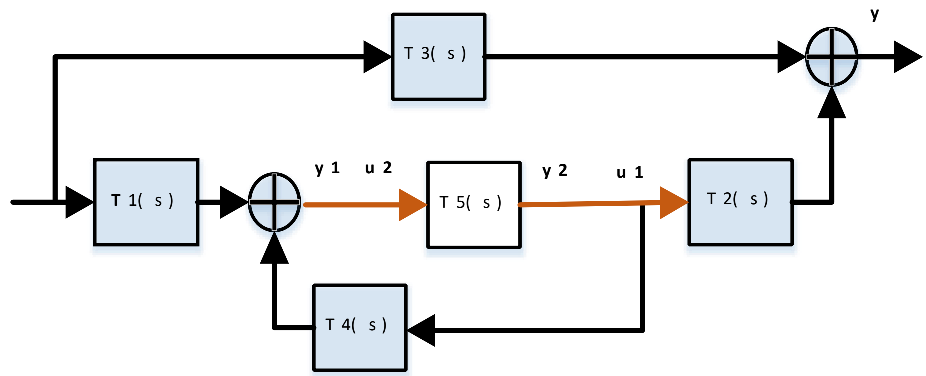

Fig. 4: Block-diagram representation for the system presented in the proof of Theorem 1.

Each transfer function T_i (i = 1,…,4) can be written as $T_i = \frac{a_i(s)}{b_i(s)}$, where $a_i(s)$ and $b_i(s)$ are the polynomials in the numerator and denominator respectively. Then,

$$T(s) = \frac{Y(s)}{U(s)}$$
$$= \frac{(H_r s^2 + D_r s + L_{r,r})b_1b_2a_3b_4 - b_1b_2a_3a_4 + a_1a_2b_3b_4}{b_1b_2b_3(b_4(H_r s^2 + D_r s + L_{r,r}) - a_4)}$$

Hence, the zeros of the input-output swing dynamics model (1) are the roots of the following equation:

$$(H_r s^2 + D_r s + L_{r,r}) b_1 b_2 a_3 b_4 - b_1 b_2 a_3 a_4 + a_1 a_2 b_3 b_4 = 0 \qquad (5)$$

Let us define $\beta_h(s) = s^2 b_1 b_2 a_3 b_4$ and $\alpha_h(s) = (D_r s + L_{r,r})\, b_1 b_2 a_3 b_4 - b_1 b_2 a_3 a_4 + a_1 a_2 b_3 b_4$. Then, the zeros equation (5) can be written as $\alpha_h(s) + H_r\beta_h(s) = 0$. Thus, the locations of the zeros in the complex plane as H_r is ranged over $[0,\infty)$ is a root locus.

Completing the proof requires some graph-theoretic analysis. In the network graph Γ, let $d_1 = d_{ir}$ be the distance from vertex i (actuated vertex) to vertex r, $d_2 = d_{rj}$ be the distance from vertex r to vertex j (measured vertex), and d_4 be the length of the shortest directed cycle containing vertex r. In addition, let $d_3 = d_{ij}^{(r)}$ be the distance from vertex i to vertex j in the deletion graph $\Gamma^{(r)}$. Based on the Theorem 1 in [9], the relative degree of the transfer functions T_1, T_2, T_3, T_4, and T_5 are equal to $2d_1$, $2d_2 - 1$, $2d_3 + 1$, $2d_4 - 2$, and 2 respectively, and all of them have positive gain.

Noting that $d_3 = d_{ij}^{(r)} \neq d_{ij}$ is considered in deleted graph $\Gamma^{(r)}$. When $d_{ij} \neq d_{ij}^{(r)}$, it is concluded that d_{ij} =

d_1+d_2, so $d_{ij}^{(r)} \geq d_{ij}+2$ can be written as $d_3 \geq d_1+d_2+2$. One can easily prove that $\deg(\alpha_h) = \deg(a_1a_2b_3b_4)$, and $\deg(\beta_h) \leq \deg(a_1a_2b_3b_4) - 3$ when $d_{ij}^{(r)} \geq d_{ij}+2$ where deg() is the degree of a polynomial. Hence, $\deg(\alpha_h(s)) \geq \deg(\beta_h(s)) + 3$.

Thus, based on root locus analysis, the zeros of the closed-loop system (5) has at least three diverging branches; two of them have asymptote in the ORHP. It follows that for sufficiently large H_r, the network input-output model has zeros in the ORHP. ■

Proof of Theorem 2: For this proof, we consider the same subsystems and notation used in the proof of Theorem 1. Let us define $\beta_d(s) = sb_1b_2a_3b_4$ and $\alpha_d(s) =$

$(H_r s^2 + L_{r,r})b_1 b_2 a_3 b_4 - b_1 b_2 a_3 a_4 + a_1 a_2 b_3 b_4$. Then, the zeros equation (5) can be written as $\alpha_d(s) + D_r\beta_d(s) = 0$. Thus, the locations of the zeros in the complex plane as D_r is ranged over $[0,\infty)$ is a root locus.

Noting that $d_3 = d_{ij}^{(r)} \neq d_{ij}$ is considered in deleted graph $\Gamma^{(r)}$. When $d_{ij} \neq d_{ij}^{(r)}$, it is concluded that $d_{ij} = d_1+d_2$, so $d_{ij}^{(r)} \geq d_{ij}+2$ can be written as $d_3 \geq d_1+d_2+2$. One can easily prove that $\deg(\alpha_d) = \deg(a_1a_2b_3b_4)$, and $\deg(\beta_d) \leq \deg(a_1a_2b_3b_4) - 4$ when $d_{ij}^{(r)} \geq d_{ij}+2$ where deg() is the degree of a polynomial. Hence, $\deg(\alpha_d(s)) \geq \deg(\beta_d(s)) + 4$.

Thus, based on root locus analysis, the zeros of the closed-loop system (5) has at least four diverging branches; two of them have asymptote in the ORHP. It follows that for sufficiently large D_r, the network input-output model has zeros in the ORHP. ■

Proof of Theorem 3: For this proof, we consider the same subsystems and notation used in the proof of Theorem 1. Let us define $\beta_l(s) = b_1b_2a_3b_4$ and $\alpha_l(s) =$

$(H_r s^2 + D_r s)b_1 b_2 a_3 b_4 - b_1 b_2 a_3 a_4 + a_1 a_2 b_3 b_4$. Then, the zeros equation (5) can be written as $\alpha_d(s) + L_{r,r}\beta_d(s) = 0$. Thus, the locations of the zeros in the complex plane as $L_{r,r}$ is ranged over $[0,\infty)$ is a root locus.

Noting that $d_3 = d_{ij}^{(r)} \neq d_{ij}$ is considered in deleted graph $\Gamma^{(r)}$. When $d_{ij} \neq d_{ij}^{(r)}$, it is concluded that $d_{ij} =$
d_1+d_2, so $d_{ij}^{(r)} \geq d_{ij}+1$ can be written as $d_3 \geq d_1+d_2+1$. One can easily prove that $\deg(\alpha_d) = \deg(a_1a_2b_3b_4)$, and $\deg(\beta_d) \leq \deg(a_1a_2b_3b_4) - 3$ when $d_{ij}^{(r)} \geq d_{ij}+1$ where deg() is the degree of a polynomial. Hence, $\deg(\alpha_d(s)) \geq \deg(\beta_d(s)) + 3$.

Thus, based on root locus analysis, the zeros of the closed-loop system, i.e. roots of (5), has at least four diverging branches; two of them have asymptote in the ORHP. It follows that for sufficiently large $L_{r,r}$, the network input-output model has zeros in the ORHP. ■

Proof of Theorem 4: For this proof, we consider the same subsystems and notation used in the proof of Theorem 1. Let us define $\beta_h(s)=s^2b_1b_2a_3b_4$ and $\alpha_h(s) =$

$(Drs + Lr,r)b_1 b_2 a_3 b_4 - b_1 b_2 a_3 a_4 + a_1 a_2 b_3 b_4$. Then, the zeros equation (5) can be written as $\alpha_h(s) + H_r\beta_h(s) = 0$. Thus, the locations of the zeros in the complex plane as H_r is ranged over $[0,\infty)$ is a root locus.

When $d_{ij} = d_{ij}^{(r)}$, it is concluded that $d_{ij} \leq d_1 + d_2$, one can easily show that $\deg(\beta_h(s)) = \deg(\alpha_h(s))+1$. Thus, based on root locus analysis, for sufficiently large gain H_r (i.e. as H_r is scaled up), the zeros of the closed-loop transfer function are arbitrary close to the roots of $\beta(s)$. Further, the roots of $b_1(s)$, $b_2(s)$, and $b_4(s)$ are in OLHP because the subsystem C_1 in (3) is internally stable. Meanwhile, $a_3(s)$ is the numerator of the transfer function $T_3(s) = \frac{Y(s)}{U(s)}$, and hence its roots are the zeros of the input-output model (2). In conclusion, if the removal of vertex r does not change the distance from input to output in the network graph, then two of the zeros of (1) approach the origin $s = 0$, the remaining zeros either approach the zeros of the modified system (2) or are in OLHP, as the inertia H_r is scaled up. ■

Proof of Theorem 5: For this proof, we consider the same subsystems and notation used in the proof of Theorem 1. Let us define $\beta_d(s) = sb_1b_2a_3b_4$ and $\alpha_d(s) =$ $(H_r s^2 + L_{r,r})b_1 b_2 a_3 b_4 - b_1 b_2 a_3 a_4 + a_1 a_2 b_3 b_4$. Then, the zeros equation (5) can be written as $\alpha_d(s) + D_r\beta_d(s) = 0$. Thus, the locations of the zeros in the complex plane as D_r is ranged over $[0,\infty)$ is a root locus.

When $d_{ij} = d_{ij}^{(r)}$, it is concluded that $d_{ij} \leq d_1 + d_2$, one can easily show that $\deg(\alpha_d(s)) = \deg(\beta_d(s)) + 1$. Thus, based on root locus analysis, for sufficiently large gain D_r (i.e. as D_r is scaled up), one of the zeros of the closed-loop transfer function is in OLHP (far from imaginary axis) and the remaining zeros are arbitrary close to the roots of $\beta(s)$. Further, the roots of $b_1(s)$, $b_2(s)$, and $b_4(s)$ are in OLHP because the subsystem C_1 in (3) is internally stable. Meanwhile, $a_3(s)$ is the numerator of the transfer function $T_3(s) = \frac{Y(s)}{U(s)}$, and hence its roots are the zeros of the input-output model (2). In conclusion, if the removal of vertex r does not change the distance from input to output in the network graph, then one the zeros of (1) approaches the origin $s = 0$, the rest either approach the zeros of the modified system (2) or are in OLHP, as the inertia D_r is scaled up. ■

Proof of Theorem 6: Consider $V_{\{ij\}}$ as the set of all numbers from set $\{1,2,\cdots,n\}$ except the numbers i and j. Also considering a general matrix B with dimension (n,n), matrix $\bar{B} = B^{(V\{ij\})}$ is defined as a submatrix of B obtained by deleting the rows and columns not specified in $V_{\{ij\}}$. Considering the adjacent input and output vertices and by using the results from Theorem 2 in [9], one can easily show that the corresponding matrices A_{na} and A_q are equal to $A_{na} = \begin{bmatrix} 0 & I \\ -\bar{H}^{-1}\bar{L} & -\bar{H}^{-1}\bar{D} \end{bmatrix}$ and $A_q = \begin{bmatrix} 0 & 0 \\ -\bar{H}^{-1}\bar{M} & 0 \end{bmatrix}$ where $M = L_{i,j}^{-1}\bar{L}_{:,i}\bar{L}_{j,:}$. Hence the matrix A_{aa} is equal to $A_{aa} = \begin{bmatrix} 0 & I \\ -\bar{H}^{-1}W & -\bar{H}^{-1}\bar{D} \end{bmatrix}$ where $W = \bar{L} + M$.

Let us define matrix $T = \begin{bmatrix} I & \bar{D}^{-1}\bar{H} \\ 0 & I \end{bmatrix}$. The eigenvalues of matrix $TA_{aa}T^{-1}$ =

$$\begin{bmatrix} -\bar{D}^{-1}\bar{W} & \bar{D}^{-1}\bar{W}\bar{D}^{-1}\bar{H} \\ -\bar{H}^{-1}\bar{W} & \bar{H}^{-1}\bar{W}\bar{D}^{-1}\bar{H} - \bar{H}^{-1}\bar{D} \end{bmatrix}$$

are equal to the eigenvalues of A_{aa}.

We know that the zeros of the input-output swing-dynamics model (1) are the eigenvalues of matrix $TA_{aa}T^{-1}$, sobBased on Gersgorin's disk theorem to keep the eigenvalues of $TA_{aa}T^{-1}$ in OLHP, we can write inequalities that are in the theorem statement.

■

Proof of Theorem 7: Based on the discussion in the proof for Theorem 4 in [9], the perturbation matrix A_q is zero, hence $A_{aa} = A_{na}$. Consider $V_{\{i\}}$ as the set of all numbers from set $\{1,2,\cdots,n\}$ except the number i. Considering a general matrix B with dimension (n,n), matrix $\bar{B} = B^{(V\{i\})}$ is defined as a submatrix of B obtained by deleting the rows and columns not specified in V_i. Then the matrix A_{aa} is equal to $A_{aa} = \begin{bmatrix} 0 & I \\ -\bar{H}^{-1}\bar{L} & -\bar{H}^{-1}\bar{D} \end{bmatrix}$. Let us define

The matrix $T = \begin{bmatrix} I & \bar{D}^{-1}\bar{H} \\ 0 & I \end{bmatrix}$. The eigenvalues of matrix A_{aa} are equal to the eigenvalues af matrix $TA_{aa}T^{-1} =$ $\begin{bmatrix} -D \quad L & D \quad LD \quad H \\ -\bar{H}^{-1}\bar{L} & \bar{H}^{-1}\bar{L}\bar{D}^{-1}\bar{H} - \bar{H}^{-1}\bar{D} \end{bmatrix}$

We know that the zeros of the input-output swing-dynamics model (1) are the eigenvalues of matrix $TA_{aa}T^{-1}$, so Based on Gersgorin's disk theorem to keep the eigenvalues of $TA_{aa}T^{-1}$ in OLHP, we can write the following inequalities. The first set of inequalities are based on the first $n-1$ rows of the matrix $TA_{aa}T^{-1}$ and the second set of inequalities are based on the second $n-1$ rows as following: $\forall k \neq i$:

$$2\,|L_{kk}| \geq \sum_{m \neq i} \frac{D_m + H_m}{D_m}\,|L_{km}|$$

$$D_k \geq \sum_{m \neq i} \frac{D_m + H_m}{D_m}\,|L_{km}|$$

References

[1] Y. Zhang and A. Bose, "Design of wide-area damping controllers for interarea oscillations," IEEE Transactions on Power Systems, vol. 23, no. 3, pp. 1136–1143, 2008.

[2] A. Chakrabortty and P. P. Khargonekar, "Introduction to wide-area control of power systems," in American Control Conference (ACC), 2013. IEEE, 2013, pp. 6758–6770.

[3] P. Korba, E. Scholtz, A. Leirbukt, and K. Uhlen, "Combining forces to provide stability," ABB Review, vol. 3, pp. 34–38, 2007.

[4] A. Ulbig, T. S. Borsche, and G. Andersson, "Analyzing rotational inertia, grid topology and their role for power system stability," IFAC-PapersOnLine, vol. 48, no. 30, pp. 541–547, 2015.

[5] K. Koorehdavoudi, S. Roy, J. A. Torres, and M. Xue, "Interactions among control channels in dynamical networks," in Decision and Control (CDC), 2017 IEEE 56th Annual Conference on. IEEE, 2017, pp. 1058–1063.

[6] S. Skogestad and I. Postlethwaite, Multivariable feedback control: analysis and design. Wiley New York, 2007, vol. 2.

[7] F. Dorfler, M. Chertkov, and F. Bullo, "Synchronization in complex oscillator networks and smart grids," Proceedings of the National Academy of Sciences, vol. 110, no. 6, pp. 2005–2010, 2013.

[8] M. Pirani, J. W. Simpson-Porco, and B. Fidan, "System-theoretic performance metrics for low-inertia stability of power networks," in Decision and Control (CDC), 2017 IEEE 56th Annual Conference on. IEEE, 2017, pp. 5106–5111.

[9] K. Koorehdavoudi, M. Hatami, S. Roy, V. Venkatasubramanian, P. Panciatici, F. Xavier, and J. A. Torres, "Input-output characteristics of the power transmission network's swing dynamics," in Decision and Control (CDC), 2016 IEEE 55th Conference on IEEE, 2016, pp. 1846–1852.

[10] K. Koorehdavoudi, S. Roy, T. Prevost, F. Xavier, P. Panciatici, and V. M. Venkatasubramanian, "Input-output properties of the swing dynamics for power transmission networks with hvdc modulation," IFAC-PapersOnLine, vol. 50, no. 1, pp. 5442–5447, 2017.

[11] K. Koorehdavoudi, M. Yao, S. Roy, and J. L. Mathieu, "Using demand response to shape the fast dynamics of the bulk power network," in Proceedings of the IREP Symposium on Bulk Power System Dynamics and Control, Espinho, Portugal, 2017.

[12] M. Mesbahi and M. Egerstedt, Graph theoretic methods in multi-agent networks. Princeton University Press, 2010.

[13] F. Pasqualetti, S. Zampieri, and F. Bullo, "Controllability metrics, limitations and algorithms for complex networks," IEEE Transactions on Control of Network Systems, vol. 1, no. 1, pp. 40–52, 2014.

[14] R. Dhal and S. Roy, "Vulnerability of continuous-time network synchronization processes: A minimum energy perspective," in Decision and Control (CDC), 2013 IEEE 52nd Annual Conference on. IEEE, 2013, pp. 823–828.

[15] C. B. Schrader and M. K. Sain, "Research on system zeros: a survey," International Journal of control, vol. 50, no. 4, pp. 1407–1433, 1989.

[16] J. van der Woude, "The generic number of invariant zeros of a structured linear system," SIAM Journal on Control and Optimization, vol. 38, no. 1, pp. 1–21, 1999.

[17] B. Briegel, D. Zelazo, M. Burger, and F. Allgower, "On the zeros of consensus networks," in Decision and Control and European Control Conference (CDC-ECC), 2011 50th IEEE Conference on. IEEE, 2011, pp. 1890–1895.

[18] I. Herman, D. Martinec, and M. Sebek, “Zeros of transfer functions in networked control with higher-order dynamics,” IFAC Proceedings Volumes, vol. 47, no. 3, pp. 9177–9182, 2014.
[19] J. Abad Torres and S. Roy, “Graph-theoretic characterisations of zeros for the input–output dynamics of complex network processes,” International Journal of Control, vol. 87, no. 5, pp. 940–950, 2014.
[20] J. A. Torres and S. Roy, “Graph-theoretic analysis of network input–output processes: Zero structure and its implications on remote feedback control,” Automatica, vol. 61, pp. 73–79, 2015.
[21] K. Koorehdavoudi, S. Roy, J. A. Torres, and M. Xue, “Impacts of high and low gain controllers on remote channels in dynamical networks,” in 2018 IEEE Conference on Decision and Control (CDC). IEEE, 2018, pp. 3680–3685.
[22] ——, “Influence of diffusive-network controllers on remote channel zeros,” in preparation.
[23] K. Koorehdavoudi, S. Roy, and M. Xue, “Distributed decision-making algorithms with multiple manipulative actors: A feedback-control perspective,” in 2018 IEEE Conference on Decision and Control (CDC). IEEE, 2018, pp. 4439–4444.
[24] K. Koorehdavoudi, S. Roy, M. Xue, and J. A. Torres, “Interactions among heterogeneous manipulative actors in distributed decision-making processes: Static and dynamic analysis,” in 2019 Annual American Control Conference (ACC).
[25] ——, “Distributed decision-making algorithms with multiple manipulative actors,” Automatica, 2019.
[26] K. Koorehdavoudi, S. Roy, T. Prevost, F. Xavier, P. Panciatici, and V. Venkatasubramanian, “Input-output properties of the power grid’s swing dynamics: Dependence on network parameters (with proofs).”
[27] P. Kundur, N. J. Balu, and M. G. Lauby, Power system stability and control. McGraw-hill New York, 1994, vol. 7.
[28] P. W. Sauer and M. Pai, “Power system dynamics and stability,” Urbana, 1998.
[29] J. J. Sanchez-Gasca and J. H. Chow, “Power system reduction to simplify the design of damping controllers for inter-area oscillations,” IEEE Transactions on Power Systems, vol. 11, no. 3, pp. 1342–1349, 1996.
[30] M. Ostadijafari, S. Fakhimi, and M. A. Omam, “Robust cooperative saturated output feedback control of uncertain networked euler-lagrange systems,” in 2017 International Conference on Mechanical, System and Control Engineering (ICMSC). IEEE, 2017, pp. 230–234.